Molecular dynamics simulation of associative polymers: Understanding linear viscoelasticity from the sticky Rouse model

Article *in* Journal of Rheology · July 2021

DOI: 10.1122/8.0000218

4 authors, including:

Nuofei Jiang
Fudan University
4 PUBLICATIONS **6** CITATIONS

SEE PROFILE

Molecular dynamics simulation of associative polymers: Understanding linear viscoelasticity from the sticky Rouse model

Nuofei Jiang, Hongdong Zhang, Yuliang Yang, and Ping Tang

Citation: Journal of Rheology **65**, 527 (2021); doi: 10.1122/8.0000218
View online: https://doi.org/10.1122/8.0000218
View Table of Contents: https://sor.scitation.org/toc/jor/65/4
Published by the The Society of Rheology

Molecular dynamics simulation of associative polymers: Understanding linear viscoelasticity from the sticky Rouse model

Nuofei Jiang, Hongdong Zhang, Yuliang Yang, and Ping Tang[a)]

State Key Laboratory of Molecular Engineering of Polymers, Department of Macromolecular Science, Fudan University, Shanghai 200433, China

(Received 4 January 2021; final revision received 1 May 2021; published 24 May 2021)

Abstract

Polymers bearing associative groups (APs) are characterized by their fantastic viscoelastic behaviors. In a work recently published by our group [Jiang *et al.*, *Macromolecules* **53**, 3438–3451 (2020)], a single chain sticky Rouse model (SRM) is proposed to describe the linear viscoelasticity of APs without the entanglement effect. In this work, equilibrium molecular dynamics simulation of an unentangled melt of an AP with uniformly distributed stickers is carried out, and the dynamic properties are simultaneously analyzed from the SRM. A chain model with capped stickers is proposed so that a well-defined association chemistry is promised in the simulation system. The relative effective frictional coefficient of stickers, which is the key parameter in the SRM, is extracted from the chain center-of-mass diffusion, and it is found to be consistent with the dynamics of associative reaction in the fully gelated network. Based on this, a linear relaxation modulus and segmental diffusion functions are predicted from the SRM without fitting parameters, and these are found to quantitatively agree with the simulation results, showing the effectiveness of the SRM in connecting the dynamic properties at different molecular levels. The change in relaxation modes and the definition of the effective chain center are found to be crucial in the scenario of the SRM. Finally, the above analysis from the SRM is successfully extended to the simulation system with asymmetric chains. All these simulation results strongly support the SRM as a molecular model for the linear rheology of AP. https://doi.org/10.1122/8.0000218

I. INTRODUCTION

Polymers bearing stickers, which can reversibly associate with each other through noncovalent interactions, such as hydrogen bonding, π-π stacking, van der Waals interactions, or metal-ligand coordination interactions, are not only widely used as functional materials [1–3], but also can exhibit fascinating viscoelastic behaviors [4–6]. These associative polymers (APs) are very sensitive to external conditions like temperature and flow fields, and even an extremely small change in the amount of sticky motifs will greatly tune the bulk properties. In order to better explain the complex viscoelastic behaviors and exploit the potential applications of APs, a thorough understanding of the role of associative interaction at the molecular level is needed.

It usually recognized that APs should follow a so-called "sticky Rouse" dynamics [7,8] in the unentangled regime and "sticky reptation" [9,10] or "living reptation" dynamics [11] in the entangled regime, compared with the classic Rouse and reptation dynamics for a homopolymer system. In most of the literature, the term "sticky Rouse" refers to a kind of hierarchal dynamics that is separated by the length scale of the strand between stickers. Below this scale is the unaffected Rouse motions of non-sticky segments. Above this scale, the strands will serve as some sub-springs connecting the n_s sticky beads, where n_s is the number of stickers in a single chain so that the Rouse-like dynamics reappears. Therefore, the relaxation modes are divided into two groups, a fast group and a slow group. The divergence of the two relaxation groups caused by the strength of associative interaction finally leads to an elastic plateau regime in the modulus. The Rouse-like dynamics of APs on a large scale was first reported by Baxandall [12], who derived the dynamics from the probability distribution function in configurational space. In a later work, Rubinstein and Semenov [8] proved the sticky Rouse dynamics from the scaling approach, by introducing a so-called effective breakup time, wherein a large aggregate breaks into two parts of comparative size. This approach is found to be extremely useful in explaining the scaling behaviors near the gelation point [13]. Except for these widely noticed works, the sticky Rouse dynamics is also found in some other models, like the statistic models proposed by Wientjes and co-workers [14,15], and by Indei and Takimoto [16].

Although the proof of sticky Rouse dynamics has successfully explained the rheological data observed in experiments, it is still hard to claim that these concepts are serving as a molecular model like the classic Rouse model, because the effectiveness of the classic Rouse model is not limited to predicting these macroscopic properties. The Rouse model also points out the connections between the polymer rheology and some other microscopic functions, including the dynamic structure factor and the orientational correlation function of bond vectors [17]. The latter is the core function of dielectric relaxation in polymers with type-A dipoles [18]. The effectiveness of the Rouse model can also be judged by the fact that it can be directly applied to any chain topologies by simply modifying the connectivity between a pair of beads. Thus, the

[a)]Author to whom correspondence should be addressed; electronic mail: pingtang@fudan.edu.cn

effect of the topological structure on rheology is also well explained by the Rouse model [19]. However, these connections are rarely mentioned by previous theories on APs. Presently, experimental data on microscopic behaviors in associative networks have been made available. For example, Olsen and co-workers [20–22] reported an anomalous self-diffusion before the Fick regime in associating protein hydrogels and explained this phenomenon from a two-state model [22]. In spite of this, its connection with the sticky Rouse dynamics has not been fully understood. Very recently, a new framework of the sticky Rouse model (SRM) was reported by our group [23], which has the potential to serve as a molecular model and bridge the gap between the micro- and macroscopic dynamics in APs. The present work will focus on its validity in this aspect.

One purpose of the present work is to prove how the SRM helps in understanding the linear viscoelasticity (LVE) of APs at the molecular level, with the support of molecular dynamics simulation results. The other purpose is to find out some missing aspects about the linear rheology of APs. The rest of the paper is organized as follows: In Sec. II, the framework of the SRM is reintroduced and the physical picture is emphasized. In Sec. III, the criteria to choose the simulation method are discussed and a simulation model with a controlled aggregation of stickers is proposed. Linear chain structures with periodically distributed stickers are selected. In Sec. IV, the static structures of the simulation system and the dynamics of associative reaction are analyzed in the first place. Then, the SRM is applied to the simulation system, which provides quantitative comparisons on the LVE functions and segmental diffusion functions between simulation results and theoretical predictions in a parameter-free style. Afterward, these discussions are further extended to the associative system with asymmetric chains. Finally, the scope of the present work is summarized in Sec. V.

II. THEORETICAL MODEL

The key idea of the SRM comes from the microscopic expression of stress. In a monodisperse bead–spring chain system, the stress $\sigma_{\alpha\beta}$ is expressed as

$$\sigma_{\alpha\beta} = \frac{3k_{\mathrm{B}}T\rho}{Nb^2}\sum_{i=2}^{N}\left\langle(\mathbf{r}_i-\mathbf{r}_{i-1})_\alpha(\mathbf{r}_i-\mathbf{r}_{i-1})_\beta\right\rangle - p\delta_{\alpha\beta}, \tag{1}$$

where $\mathbf{r}_i$ is the position of the ith segment, N is the number of beads per chain, b is the Kuhn length, $k_{\mathrm{B}}T$ is the reduced temperature, ρ is the number density of beads, and p is the isotropic pressure. This expression of stress is derived by assuming that only chain elasticity contributes to the deviatoric stress, but it is found to be widely applicable, which is strongly supported as the stress-optical law when the system is homogeneous and the applied stress is not too large [17]. It can be read from Eq. (1) that the key step in understanding the viscoelastic behavior of polymers at the molecular level is to track the Brownian motion of a single polymer chain in its surroundings. When it comes to an unentangled AP, the most intuitive physical scenario is an associative chain moving in the surroundings with some reactive sites, as shown in Fig. 1(a). When a sticker is not bonded to any sites, it behaves as a normal bead, while when it is associated with one of these sites, it becomes nearly fixed or is allowed to jump to another site after a specific timescale. In contrast to this direct physical scenario, the idea of the SRM, as shown in Fig. 1(b), is that the mobility of stickers is thought to be permanently retarded [23]. The degree of retardation relies on the dynamics of associative reaction and can be described as an effective frictional force acting on stickers. At the same time, the surroundings can be regarded as a homogeneous medium, because the effect of the reactive sites has been enclosed into the effective friction. Through this indirect treatment, the formulation of the single-chain Brownian dynamics is significantly simplified, because it can be directly developed from the classic Rouse model [24] by introducing mobility heterogeneity. In addition, all these advantages of the Rouse model will be inherited, which brings a clearer molecular picture to the structure–property relationship in APs.

By referring to the work of Hansen and Shen [25], the single chain dynamics is formulated from the following matrix form of the Langevin equation:

$$\xi\boldsymbol{\Xi}\frac{\mathrm{d}\mathbf{Q}}{\mathrm{d}t} = -\frac{3k_{\mathrm{B}}T}{b^2}\mathbf{Z}\mathbf{Q} + \mathbf{F}, \tag{2}$$

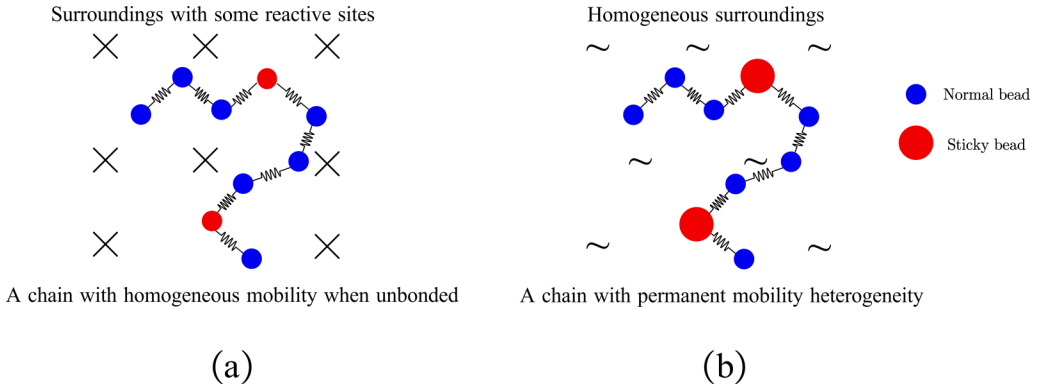

FIG. 1. Two types of description for an associative chain and its surroundings in an associative system. (a) There are some reactive sites in the surroundings. The reactive beads in the labeled chain share the same mobility with normal beads when unbonded, while becoming nearly fixed when bonded; (b) the labeled chain is in the homogeneous surroundings, while the mobility of sticky beads is permanently retarded.

where ξ is the background frictional coefficient. It is a mean-field substitute for the hypothetic homogeneous surroundings. $\mathbf{Q}$ is the column vector of segment positions. $\mathbf{Z}$ is the Rouse–Zimm (RZ) matrix that describes the connectivity between beads. For a linear chain, it is

$$\mathbf{Z} = \begin{bmatrix} 1 & -1 & & \\ -1 & 2 & -1 & \\ & & \ddots & \\ & & -1 & 1 \end{bmatrix}. \tag{3}$$

$\mathbf{F}$ is the random force term that satisfies the fluctuation–dissipation correlation. Compared with the classic Rouse model, a new diagonal matrix $\boldsymbol{\Xi}$ is introduced to describe the mobility heterogeneity,

$$\boldsymbol{\Xi} = \begin{bmatrix} \delta_1 & & & \\ & \delta_2 & & \\ & & \ddots & \\ & & & \delta_N \end{bmatrix}, \tag{4}$$

where $\delta_i = \xi_i/\xi$ is the relative frictional coefficient for the ith segment. For a non-sticky segment, $\xi_i/\xi = 1$. For a sticker, $\delta = \xi_s/\xi \gg 1$ stands for the enhanced dragging effect caused by association. By introducing normal coordinates $\mathbf{X}_p$, where $p = 0, 1, \ldots, N-1$, Eq. (2) can be rewritten into a group of independent equations,

$$\xi \frac{\partial}{\partial t}\mathbf{X}_p = -\frac{3k_B T\lambda_p}{b^2}\mathbf{X}_p + f_p, \tag{5}$$

where $0 = \lambda_0 < \lambda_1 \cdots < \lambda_{N-1}$ are the eigenvalues of the so-called sticky RZ matrix $\boldsymbol{\Xi}^{-1}\mathbf{Z}$. The time correlation function of the normal coordinate is then obtained as

$$\left\langle X_{p\alpha}(t)X_{q\beta}(0)\right\rangle = \delta_{pq}\delta_{\alpha\beta}\frac{\tau_p\left\langle f_{p\alpha}f_{q\beta}\right\rangle}{\xi^2}\exp(-t/\tau_p) \qquad \text{for } p > 0, \tag{6}$$

where

$$\tau_p = \frac{\tau_0}{\lambda_p} \tag{7}$$

and

$$\tau_0 = \frac{\xi b^2}{3k_B T}. \tag{8}$$

Using the inverse form of normal transformation,

$$\mathbf{r}_i = \sum_{p=0}^{N-1} v_i^p \mathbf{X}_p, \tag{9}$$

where v_i^p is the ith element of the pth eigenvector of $\boldsymbol{\Xi}^{-1}\mathbf{Z}$, Eq. (1) is rewritten as

$$\sigma_{\alpha\beta} = \frac{3k_B T\rho}{Nb^2}\sum_{p=0}^{N-1}\sum_{i=2}^{N}\left(\frac{\mathrm{d}v_i^p}{\mathrm{d}i}\right)^2\left\langle X_{p\alpha}X_{p\beta}\right\rangle - p\delta_{\alpha\beta}, \tag{10}$$

which will finally lead to the molecular expression of LVE functions, including the linear relaxation modulus $G(t)$, the dynamic modulus $G'(\omega)$ and $G''(\omega)$, the zero-shear viscosity η_0, and the steady-state recoverable compliance J_e^0. From the above friction-based approach, it is found [23] that the characteristics of sticky Rouse dynamics are naturally raised. The eigenvalues λ_p are directly separated into two groups by increasing the values of δ when $n_s \geq 2$, with a reasonable transition from the Rouse to the sticky Rouse behavior. In addition, the analysis on eigenvectors indicates there shall be a change in relaxation behavior at the segmental level. For example, the longest relaxation time can be related to the rotational motion of the network strand.

In order to prove the validity of the SRM, not only the macroscopic LVE but also the microscopic dynamic properties are required. In this case, a molecular dynamics (MD) simulation shall be the best choice. Up to now, some simulation studies on the viscoelastic properties of APs have been reported [26–32]. Also, several mechanisms have been proposed to connect the dynamics at the microscopic and macroscopic levels. For example, Hoy and Fredrickson [27] investigated the detailed chemical dynamics in APs and identified the kinetically limited and diffusion-limited association behaviors in them. Amin *et al.* [28] proposed a partner exchange mechanism on how an associated structure relaxed and found that this mechanism is more favored than the conventional sticker hopping process. Despite these efforts, we are still far away from carrying out a thorough discussion about the SRM.

III. SIMULATION METHOD

In the present work, the choice of the simulation method is based on the theoretical background of the SRM. Like the classic Rouse model, the SRM does not consider the effect of excluded volume interactions and hydrodynamics. In addition, it has been assumed that all stickers are equally associated and all associative chains are identical. Such a description is closer to a dense melt of APs. The best choice for us is to refer to the classic Kremer–Grest model simulation [33]. The Kremer–Grest model is a coarse-grained bead–spring model and has been used in investigating a variety of properties of polymers, especially the entanglement effect in polymer melts. In this model, the pairwise interaction between beads is the WCA style Lennard–Jones (LJ) potential,

$$U_{\mathrm{LJ}}(\mathrm{r}) = \begin{cases} 4\varepsilon\left[\left(\frac{\sigma}{r}\right)^{12} - \left(\frac{\sigma}{r}\right)^{6}\right] - U_{\mathrm{LJ}}(r_c) & r \leq r_c, \\ 0 & r > r_c, \end{cases} \tag{11}$$

where the cutoff distance is set to $r_c = 2^{1/6}$ (at LJ unit. The description of LJ units is listed in Table S1 [89]). Thus, only the repulsive part of the pair interaction is considered. The bond potential is the finite extensible nonlinear elastic (FENE) style,

$$U_{\mathrm{FENE}} = -\frac{k}{2}R_0^2 \ln\left[1 - \left(\frac{r}{R_0}\right)^2\right], \tag{12}$$

where $R_0 = 1.50$ and $k = 30$. The angle potential is not considered in the present work. A typical Kremer–Grest model simulation for an equilibrated melt is conducted with the following settings: a Langevin thermostat $m\ddot{\mathbf{r}}_n = -\nabla U - \zeta\dot{\mathbf{r}}_n + \boldsymbol{f}_n$ with the damp parameter $\zeta = 0.5$, a constant number density of monomers $\rho = 0.85$, reduced temperature $k_{\mathrm{B}}T = 1.0$, and upgrading position and velocity with a time step $\Delta t = 0.01$. The simulation box can be equilibrated via the strategy proposed by Auhl *et al.* [34] before sampling the thermodynamic properties.

In order to mimic associative interactions in APs, the simplest strategy, as has been used by some other simulation works [30,31], is to set a certain number of backbone monomers as stickers and change the LJ pair cutoff distance between the stickers to $r_{\mathrm{c}}' = 2.5$ so that there will be an attractive potential between them, as shown in Fig. 2(a). The depth of the potential well will stand for the association energy ε_{a}. Meanwhile, the interaction between stickers and other non-sticky monomers remains to be of the pure repulsive style. This type of association interaction has two characteristics: one is that only the dissociation process has an activation energy, but the association process does not; the other is an uncontrollable tendency of sticker aggregation. Indeed, the aggregate of stickers, which is called "cluster" in the rest of the paper, is an important structure in real APs [35–37]. They behave as multiple functional crosslinkers to provide the mechanical properties of APs. These cluster structures have also been frequently reported by previous simulations [30,31,38–42]. In some cases where the amount of associative groups is very large [39–41], the stickers can even form a percolated phase. Considering this fact, a modified model or another method to model association is needed in this work to control the clustering effect because of the following two reasons: one is that the theoretical foundation of the SRM is the ideal form of stress in Eq. (1), which is supported only in the presence of a spatial homogeneity and a limited amplitude of stress. A large cluster structure will probably cause an unpredictable deviation from this expression. In a very recent work by Mordvinkin *et al.* [43], it was reported that, in the unentangled telechelic network, where poly(isobutylene) (PIB) is used as the building block and barbituric acid serves as the sticker, the single-chain relaxation is still found to be consistent with the rheological property, even though micellar clusters are formed. Such an agreement may indicate that these cluster structures have not led to an observable discrepancy from the ideal expression of stress. It can also be speculated that there might be a critical cluster size, beyond which it will be no longer plausible to predict rheological properties from the single-chain dynamics in associative systems. In the present work, it is better to minimize the deviation from Eq. (1) so that the effect from other factors can be properly analyzed. The other reason to bring the cluster size under control is to realize a well-defined association chemistry so that the dynamics of associative reactions and the stickiness of stickers (the values of δ) can be quantitatively compared. Such a comparison will prove whether the basic assumption of the SRM is supported.

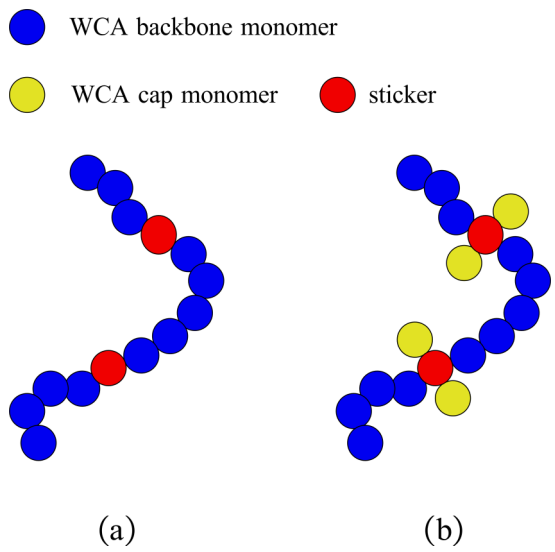

FIG. 2. Simulation models of an associative chain with (a) bald stickers and (b) stickers capped with WCA beads.

In order to control the size of a cluster, some strategies have been proposed. A prevalent one is the hybrid Monto Carlo (MC)/MD method [27–29, 44, 45], where the association and dissociation of stickers are proceeded based on MC criteria, but the motions of monomers still follow an MD style. In this paper, we introduce a capped model for APs, as shown in Fig. 2(b). In this model, backbone stickers with attractive interaction are bonded with several non-sticky cap monomers. After several stickers have been associated together, further aggregation will be hindered by the repulsion from not only the connecting monomers, but also caps. As a result, the maximum size of a cluster is controlled by the number of caps. A comparison of cluster size with different numbers of caps is presented in Fig. S1 of the supplementary material [89]. In the present work, we choose the 3-cap model and the cluster size will not exceed 5 in the range of associative energy we considered here ($\varepsilon_{\mathrm{a}} \leq 12.0$). Two typical kinds of cluster size distribution function are shown in Fig. S2 [89]. Such a maximum cluster size is very close to the aggregation number observed in ionomer polymers (5–10 ionic groups at a spacing of 3–5 nm) [46,47]. Moreover, as shown in Fig. S3 [89], the cluster size is nearly independent of the sticker's concentration, which allows a more detailed discussion on the association dynamics. This is not usually the case in hydrogen bonded or ionomer systems [48,49] but can be realized in APs with metallo interaction [50]. With such an implementable model, we will be able to keep our discussions on the homogeneous condition combined with well-controlled chemical structures.

In the present simulation work, we will first discuss a specific case of AP, where linear AP chains have a fixed molecular weight with stickers periodically distributed along the backbone, as has been theoretically analyzed in our previous paper [23]. In this case, we can focus on only two association parameters: the number of stickers per chain n_{s} and the association interaction energy ε_{a}. In these chain models, the

stickers are strictly positioned in the contour location of $(i + 1/2)\bar{N}_s$ for $i = 0, 1, \ldots, n_s - 1$, where $\bar{N}_s = N/n_s$ is the average spacing between stickers, and it relates to the global concentration of stickers ρ_s as $\rho_s = \rho n_s/N = \rho/\bar{N}_s$. Thus, for 1-sticker polymers, the sticker is in the middle, while for a chain model with more than one sticker, there will be two symmetric dangling ends with a length of $\bar{N}_s/2$. In such a periodic style, the exact length of the network strand and the density of junctions are simply correlated if there is a network structure. The AP chain model has a total monomer number (backbone monomers plus cap monomers) of 60. So, the backbone lengths of the AP chains with 1–4 stickers will be 57, 54, 51, and 48, respectively. Binary mixtures of the same chain number are also considered here, which are represented as $n_s = 1.5$, 2.5, and 3.5. With a fixed chain size, the chain density is kept constant, and the mobility of the precursor chains does not suffer a significant interruption from the caps, although the backbone is slightly shortened. As shown in Fig. S4 [89], the relaxation moduli are almost identical in different chain models when the associative interaction is turned off. Each simulation box is composed of 200 chains. This is enough to eliminate the finite size effect, because we can obtain the same result after doubling the number of chains. In addition, the backbone length is lower than the entanglement length (around 68 estimated by primitive path analysis [51] and rheological simulations [52]), so the entanglement effect is completely trivial in the present simulation. The initial snapshots of the simulation box are prepared in LAMMPS and data-gathering runs are performed in the GPU accelerated HOOMD-blue package [53,54]. Error bar means the average of at least three independent runs from different initial snapshots.

IV. RESULT AND DISCUSSION

A. Static properties: Phase diagram of gelation and distribution of conformations

In the first place, two static properties that have a direct impact on the dynamic properties of APs are discussed: the state of gelation and the distribution of chain conformations. Both properties are dynamically balanced and reach a steady state when fully equilibrated. Gelation is a significant characteristic in an associative system, and the associative chains behave differently before and after the gelation point. As has been pointed out by the mean-field theory of gelation [6,55] and also captured by the SRM, three states of AP can be identified when screening the association parameters: the SOL where only isolated chain aggregates are formed even if the association interactions are present; the full GEL where the system is completely percolated and all chains are geometrically connected by a single giant network; the SOL + GEL that is a mixture of a network and small aggregates. Based on this geometric criterion and the numerical method described in Sec. S3 [89], the phase diagram of AP is characterized. The SOL + GEL state is identified when the giant network connects more than half of the chains. As can be seen in Fig. 3, the phase diagram is completely consistent with what has been expected. The 1-sticker AP is always an SOL regardless of the strength of association, while it is possible to find a fraction of

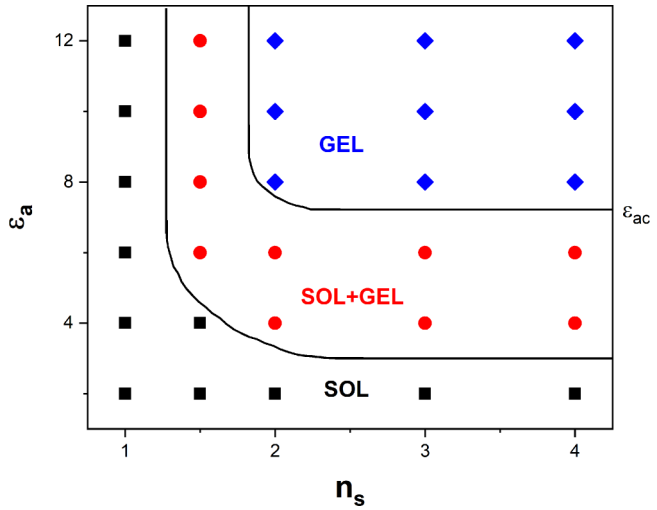

FIG. 3. Phase diagram of a simulated AP characterized from the geometrical percolation state.

the GEL component when the AP chains bear more than one sticker. Meanwhile, the predicted full gelation process from SOL to SOL + GEL and then to GEL can only be observed beyond a threshold value of the association energy ε_{ac} due to the need for effective association structures. Based on ε_{ac}, the system can be classified into strongly and weakly associated regimes. Evidently, gelation can also be triggered by increasing the association interaction when $n_s \geq 2$. In fact, the ability to form a GEL depends on the size of a cluster or the functionality of a transient junction. In the vicinity of ε_{ac}, the cluster size is about 3, which is similar to the claim by Amin *et al.* [28] that a fully developed network requires a linker functionality above 3. In a particular case, if the association is allowed only in the binary style, this phase diagram shall be different. The SOL + GEL regime will be expanded. The 2-sticker polymer will no longer be a full GEL because of the possibility of the formation of a closed loop, as expected by the mean-field theory, while the larger functionality of junctions in the present simulation facilitates the formation of a percolated network.

In the strongly associated regime, the assumption that all stickers are equally associated is satisfied because only a few stickers are found to be free (<1% when $\varepsilon_a \geq 10.0$) at any snapshot. However, this does not mean that all chains are identical, because the stickers can adopt either an inter-chain association or intra-chain association, which leads to different chain conformations. These intra-chain structures are regarded as the defects of a network, and their occurrence is unavoidable even in the melt state. Apparently, these conformations should have different relaxation behaviors, which will lead to a modification to the theoretical prediction. Each conformation can be treated as a specific kind of chain topology, as has been proposed in our previous work [23]. For example, a loop conformation can be treated as a ring topology. In addition, considering the effect of chain conformation in this work will make it more straightforward to extend the SRM to the solutions of APs, where the transformation between conformations is thought to be an important factor.

In order to classify the chain conformations, we can refer to the number of clusters n_c an associative chain can span.

TABLE I. Possible conformations in a symmetric chain model with associated stickers.

[a]	$n_c = 1$	2	3	4
$n_s = 1$	[1]			
2	[(1, 2)]	[1, 2]		
3	[(1, 2, 3)]	[(1, 2), 3]	[1, 2, 3]	
		[(1, 3), 2]		
4	[(1, 2, 3, 4)]	[(1, 2, 3), 4]	[(1, 2), 3, 4]	[1, 2, 3, 4]
		[(1, 2, 4), 3]	[(1, 3), 2, 4]	
		[(1, 2), (3, 4)]	[(1, 4), 2, 3]	
		[(1, 3), (2, 4)]	[1, (2, 3), 4]	
		[(1, 4), (2, 3)]		

[a]The numbers in the table denote the index of stickers. The round brackets denote that the enclosed stickers are in the same cluster.

All possible conformations with $n_s = 1$ to 4 are listed in Table I, given that all stickers have been bonded and the polymer chains are symmetric. The values of n_c can vary from 1 to n_s. Considering the connecting styles when there are intra-chain associations, the total number of possible conformations grows dramatically with n_s. The term "bridge" chain is applied to those with $n_c = n_s$, except the case of $n_s = 1$. A "loop" chain usually refers to the conformation where the two outermost stickers are bonded together. A conformation with $n_c = 1$ and $n_s > 2$ is named as a "flower" chain. When $n_c = 2$ and $n_s = 3$, there is another kind of conformation where the intra-chain association occurs between a neighboring pair ([(1, 2), 3] in Table I). We name it the "half loop" chain. For the $n_s = 4$ chain model, there are totally 11 possible conformations, so it will be too redundant to apply further terminologies.

Based on the values of n_c, the distribution functions of conformations are calculated and presented in Fig. 4. It becomes clear that there is indeed a fraction of intra-chain association structures in the simulation system. Also, the number of bridge chains is decreased with the sticker number n_s because of the shortened stand between a pair of stickers. Although all possible conformations have been found in the simulation box, most of the chains, except bridge chains, are adopting the conformations with a pair of neighboring association, including the loop chain ([(1, 2)]) in the $n_s = 2$ model, the half loop chain ([(1, 2), 3]) in the $n_s = 3$ model, and the [(1, 2), 3, 4] or [1, (2, 3), 4] chain in the $n_s = 4$ model. With the distribution functions of conformation, a so-called conformational average of a dynamic quantity $\mathcal{A}$ can be introduced as

$$\langle \mathcal{A} \rangle_c = \sum_k \alpha_k \mathcal{A}_k, \tag{13}$$

where α_k is the fraction of the kth kind of conformation. With the effect of conformation considered, a more detailed insight into the associative systems will be given.

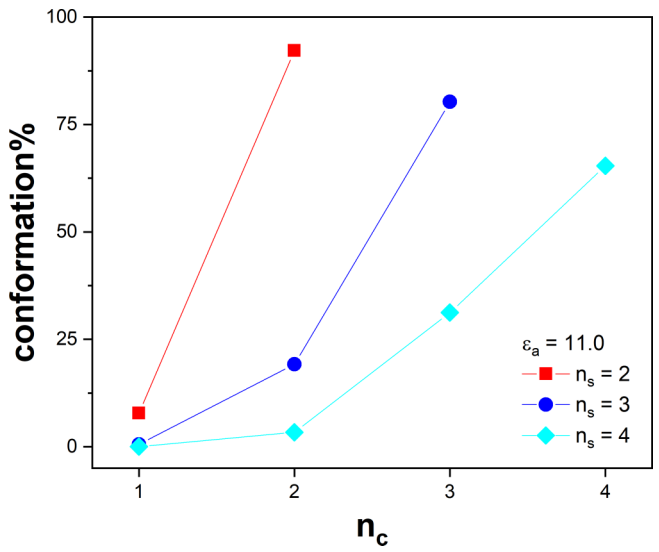

FIG. 4. Distribution function of chain conformations, classified by the number of clusters n_c that an associative chain can span.

B. Association dynamics

Before we go further into the dynamics of APs, it is necessary to make clear the association chemistry simulated by our newly proposed capped model, including the reaction style and the characteristic timescale of the associative reaction. Although there are some general properties in APs, the detailed parameter dependences rely on the certain type of association reaction. In particular, the mean lifetime of an associative bond is a more widely recognized concept and have been more frequently used in the previous theories of APs, such as the transient network theory for the nonlinear rheology of APs [56] and the scaling theory for sticky Rouse dynamics [8]. To characterize the dynamics of association in the present simulation work, we can refer to the aggregation property of stickers, because there is no actual bond between associated pairs. It can be assumed the probability P that a sticker remains in its original cluster after time Δt decays in an exponential style, that is,

$$P(\Delta t) \sim \exp(-\Delta t/\tau_{sti}), \tag{14}$$

where the partner exchange time τ_{sti} will be regarded as the effective bond lifetime or the association relaxation time. A detailed description about how τ_{sti} is calculated in the simulation is presented in Sec. S3 of the supplementary material [89]. Using this statistic method, the association dynamics is expressed in a coarse-grained style, which leaves out some detailed information in associative reactions, such as the intermediate steps of reactions. Although the importance of these intermediate steps is frequently mentioned [28,57], in this work, we are concerned about the timescale that can match with the dynamics of associative chains. Also, this coarse-grained timescale τ_{sti} is able to provide sufficient information, which will be discussed in the following sections.

As has been emphasized when we introduce the capped model, the clustering effect of stickers is controlled and the simulation system remains homogeneous in any cases. One of the consequences of such a controlling effect is found in the activation energy of association reactions. In Fig. 5, the dependence of the association time τ_{sti} on the association energy ε_a is presented. Two typical AP systems below

($n_s = 1$) and above ($n_s = 3$) the gel point are chosen. It can be seen that with the increase of ε_a, the activation energy E_a of τ_{sti} experiences a growing stage, but then becomes a constant value, showing a typical Arrhenius style relationship. This constant activation energy indicates that the coordinate number of the stickers in a cluster is not changed with ε_a, due to the limited growth of cluster size. Otherwise, the activation energy would be much more amplified, especially when some stickers are caged in the interior of clusters. Besides, the regulations of τ_{sti} in the $n_s = 1$ and $n_s = 3$ AP are very similar, which means that the associative reaction is not influenced by the gel transition. Compared with the phase diagram of Fig. 3, it is also easy to find out that the change in activation energy is consistent with the transition from the weakly to strongly associated regime. The fact that $E_a > \varepsilon_a$ in the strongly associated regime suggests that a sticker is directly bonded with more than one sticker in the same cluster. As a result, the dynamics of association and the associative structures are mutually proved.

Based on the fact that a sticker can be a part of a cluster and clusters can exchange their partners, the elementary reaction in the system can be written in the following generalized cluster/cluster reaction form:

$$(C_1 + S)^m + C_2^n \rightleftharpoons C_1^{m-1} + (C_2 + S)^{n+1}, \tag{15}$$

where C and S denote a cluster and a sticker, respectively. m and n represent the size of the clusters. The minimum size of a cluster involved in Eq. (15), $m - 1$ and n, can be zero, and a free sticker is regarded as a cluster of size 1. When $m - 1 = 0$ or $n = 0$, this chemical equation becomes the association/dissociation reaction between a sticker and a cluster pair, while when $m - 1 > 0$ and $n > 0$, Eq. (15) is the partner exchange reaction between a cluster and a cluster pair or, in other words, the hopping of a sticker from one cluster to the other. By further referring to the definition of τ_{sti} as described in Eq. (14), when $[S]$ is defined as the concentration of stickers that remains in its original cluster with the initial value $[S]_0 = \rho_s$, $[S]$ should satisfy the following dynamic equation:

$$\frac{d}{dt}([S]_0 - [S]) = -\frac{d[S]}{dt} = k_s'[C]^\beta = k_s\rho_s^\beta, \tag{16}$$

where $[C]$ is the concentration of clusters. Because the cluster size is nearly independent of the amount of stickers in the present simulation model, the ratio $\rho_s/[C]$ can be treated as a constant and is equal to the average size of a cluster. k_s is the kinetic coefficient. β is the order of the reaction. $\beta = 1$ stands for the reaction between a sticker and a cluster pair, while $\beta = 2$ denotes the hopping reaction between two clusters. When $\beta > 2$, a third cluster is thought to be involved. From the dynamic equation of Eq. (16), the relaxation of association dynamics can be expressed as

$$\begin{aligned} P(\Delta t) &= ([S]_0 + \Delta[S])/[S]_0 = 1 - k_s\rho_s^{\beta-1}\Delta t \\ &= \exp(-\Delta t/\tau_{sti}) \approx 1 - \Delta t/\tau_{sti}, \end{aligned} \tag{17}$$

where the last two terms are how the association relaxation function is fitted and its first-order expansion. Finally, we obtain the relationship between τ_{sti} and ρ_s,

$$1/\tau_{sti} = k_s\rho_s^{\beta-1}, \tag{18}$$

which will show more details about the style of associative reaction.

Based on the above demonstration, we plot the log–log relationship between τ_{sti} and ρ_s in Fig. 6. It becomes clear that, except for the activation energy, there is also a change in the reaction style when crossing from the weak to strong association regime. The value of $\beta = 1.56$ for the upper scatters, which belongs to the weakly associated regime, indicates a mixed style of reactions. The reactions between a sticker/cluster pair and a cluster/cluster pair occur simultaneously. When strongly associated, hopping becomes the dominant reaction style, because the values of β are all close to 2

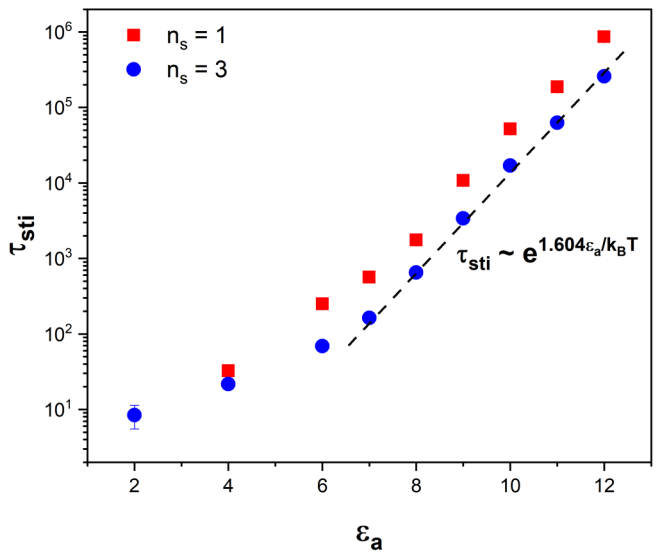

FIG. 5. Association relaxation time τ_{sti} as a function of association energy ε_a.

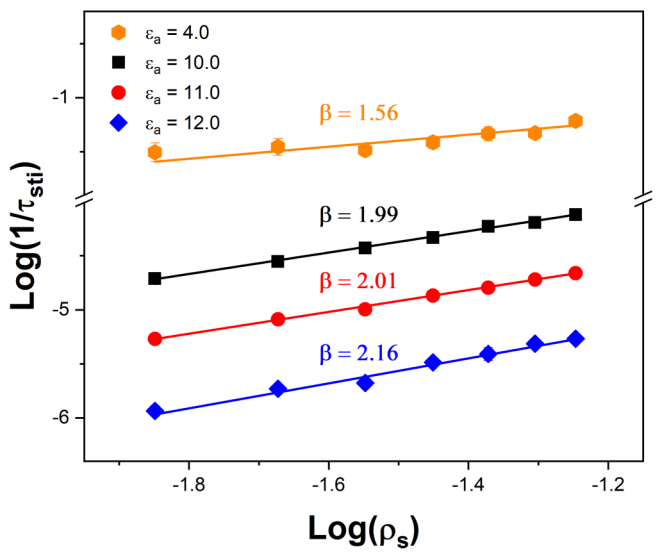

FIG. 6. Log–log relationship between τ_{sti} and ρ_s at different values of ε_a.

for $\varepsilon_a = 10.0 - 12.0$. It is also suggested that the associative reaction will be accelerated if the concentration of stickers is raised, that is, the association relaxation time τ_{sti} in the $n_s = 2$ AP is twice the value of the case of $n_s = 4$ AP. This phenomenon can be expected, because in the presence of a strong association energy, a sticker can only change its cluster number with the attraction from another clusters. Otherwise, a newly dissociated sticker will soon reassociate back to its original cluster. In addition, the size of a cluster is fixed under a certain association strength so that increasing the amount of stickers will simply increase the concentration of clusters without changing the activation energy, which finally results in a higher frequency of hopping.

From the above discussion, we can find a well-defined association chemistry in the simulation systems. The parameter dependence of τ_{sti} can be well explained from the association strength and the concentration of the reactant, without involving any chain dynamics. With a knowledge on association dynamics, it will be clear to us how the chain motions and bulk viscoelasticity are influenced by the associative interactions.

C. Effective friction from single chain diffusion

In the next step, we will investigate the relative effective frictional coefficient δ, which is one of the key parameters when predicting the LVE of APs from the SRM. Also, with the values of δ, we will be able to make a quantitative comparison between the dragging effect caused by associative interaction and the association relaxation time τ_{sti}. The relationship between these two quantities is also one of the fundamental assumptions of the SRM. The simplest way to identify the values of δ at different association parameters is from the chain center-of-mass (CM) diffusion constant D_{cm}, which can be calculated from the slope of the time-dependent mean-squared displacement (MSD) of chain CM in the Fick regime. According to the Einstein relation, without the draining of solvent, D_{cm} should be inversely proportional to the total friction force acting on a polymer chain, which is the summation of frictions on each bead. So, based on the formulation of the SRM that a sticker suffers an additional friction by a factor of δ, D_{cm} for the AP should be expressed as

$$D_{cm} = \frac{k_B T}{\sum_{i=1}^{N} \xi_i} = \frac{1}{(N - n_s) + n_s \delta} \frac{k_B T}{\xi}. \tag{19}$$

When $\delta = 1$ or $n_s = 0$, $D_{cm} = k_B T/N\xi$, which is exactly the result of the classic Rouse model. When $\delta \gg 1$, Eq. (19) can be simplified as $D_{cm} \approx k_B T/n_s \delta \xi$, indicating that the diffusion of a single chain relies mostly on the mobility of stickers. In addition, Eq. (19) can be applied to any chain topologies in the Rouse theory of diffusion, which means, even if there is a fraction of other chain conformations, the sticky friction can still be correctly calculated from D_{cm}. The expression of D_{cm} can also be derived from the normal coordinate approach in the SRM, where the zeroth normal coordinate $\mathbf{X}_0$ changes into the average position of stickers, and its dynamics is governed by the random force term in the Langevin equation. In the following section, we will introduce a so-called effective CM by weighting the friction of each bead. However, this definition will not influence the discussion in the present section, and the value of D_{cm} does not rely on how the CM is defined, because the slopes of MSD for each segment are identical in the Fick regime after all internal motions are fully relaxed.

Although the dependence of D_{cm} on n_s and δ is clear, Eq. (19) should not be directly used to extract the effective friction. The background friction coefficient ξ, which represents the surroundings for a labeled chain according to the physical picture of the SRM in Fig. 1(b), should not be treated as a constant in the present case, especially when a gelation transition can be triggered by adjusting the associative parameters. In fact, the change in surroundings has long been noticed from both experiments [58–60] and simulations [61]. For example, for *n*-paraffins with 8–60 carbons, which are completely unentangled systems, the scaling exponent a in the relationship $D_{cm} \sim N^a$ is reported to be ranging from -2.72 to -1.85 in the temperature interval from 30 to 170 °C, rather than -1 according to the prediction of the Rouse model [60]. Although this phenomenon has been explained as the free-volume and density effect, it is also plausible to regard it as a change in background friction for a labeled chain in its host matrix melts. In order to track the change of ξ, the best way is to calculate the CM diffusion constant $D_{cm/tracer}$ of some homopolymer tracer chains in the AP matrices, which do not have an associative interaction with other chains. It can be speculated that a tracer chain in the associative matrices will adopt a reptation-like dynamics because the length of the tracer can be larger than the mesh size $\bar{N}_s$. However, in the scenario of the SRM, the information that we need to know is what the surroundings should be like if it has made the labeled chain to adopt the Rouse-like diffusion. Also, because the value of the background friction will rely on the size of the tracer chain, it is necessary to have the tracer chain length strictly equal to the matrix chain. With the tracer diffusion constant, the relative frictional coefficient δ for the stickers in the matrices can be expressed as

$$\delta = \frac{N}{n_s}\left(\frac{D_{cm/tracer}}{D_{cm}} - 1\right) + 1 \approx \frac{N}{n_s}\frac{D_{cm/tracer}}{D_{cm}}, \tag{20}$$

where the approximation requires $D_{cm/tracer} \gg D_{cm}$. From the above expression, we will get the additional dragging effect on stickers caused by associative interaction, and the contribution from the non-sticky portions is also properly excluded. In the following, D_{cm} for matrix chains is obtained from the originally prepared systems, where all component chains are identical, while in order to calculate $D_{cm/tracer}$, 10 chains (accounting for 5% of the total chains) are turned into tracer chains whose stickers are changed into non-sticky segments. In this way, the introduction of tracer chains will bring only a limited effect to the matrices, but the requirement for statistics can still be met.

In the first place, the variation of the tracer chain diffusion constant $D_{cm/tracer}$ at different association parameters is

presented in Fig. 7. The corresponding profiles of MSD are presented in Fig. S6 [89]. The simulation results show that there is indeed a non-negligible change in the surroundings. With the increase in the sticker numbers per chain, the diffusion of tracer chains is greatly suppressed. The tracer diffusion in the $\varepsilon_a = 12.0$ and $n_s = 4$ matrices can be slower than that of homopolymer matrices by a factor of 4. So, the average friction acting on each segment in the tracer chains is amplified, or in other words, the hypothetic homogeneous medium becomes more viscous as the system is more densely associated. There is also a sharp change in the mobility of tracers, which is consistent with the gelation transition presented in Fig. 3. In fact, this phenomenon is predictable and has been recognized from experiments [62]. Compared with the content of stickers or the density of crosslinking of the transient network, the association energy is a less significant factor for tracer chain diffusion, because the geometric percolation state or the mesh size of the network has been fixed for the association energy presented in Fig. 7. From the above simulation results, it is proved that the change in the background friction is not a trivial factor when we try to understand the dynamics of APs from the SRM. After considering this effect, we will be able to correctly analyze the parameter dependence of δ and its relationship with the characteristics of associative reactions.

Based on Eq. (20) and the tracer diffusion behavior identified in Fig. 7, the values of δ are calculated and plotted as a function of the association relaxation time τ_{sti} in Fig. 8. The comparison shows that there is indeed a close relationship between δ and τ_{sti} in associative networks. All the scatters for AP systems with $2 \leq n_s \leq 4$ and $10.0 \leq \varepsilon_a \leq 12.0$ fall into a master curve despite the difference in chain models and association parameters. Moreover, this master curve for δ and τ_{sti} is nearly a linear function, which means that the two quantities are interchangeable and the related assumption of the SRM is strongly supported in the GEL regime. Based on this correlation, the Arrhenius relationship of τ_{sti} found in Fig. 5 is extended to δ, that is, $\delta \sim \tau_{sti} \sim \exp(E_a/k_BT)$, which suggests that δ can be manipulated in a wide numerical range in associative systems. Experimentally, this manipulation can be realized by changing the number of hydrogen bonds in reactive groups [63] or by choosing a different type of cation in ionomers [64]. In contrast to the associative systems, when the friction-modified Rouse model was originally applied to the miscible block copolymer system, δ was not an adjustable parameter ($\delta \approx 185$ for a α-methylstyrene monomer relative to a styrene monomer [25]). Although the single chain dynamics are formulated from the same equation, the physical pictures of the two systems are different. In particular, the effect of chain conformations will not appear in miscible copolymers, while it does play a role in associative systems.

Another consistence between δ and τ_{sti} is the concentration dependence, which is amplified in Fig. 9. At a constant association energy, δ is a decreasing function of n_s in the GEL regime, which is consistent with the accelerated hopping reactions found in Fig. 6. This fact further proves that hopping should be the dominant mechanism of diffusion in the present associative networks, which means that a sufficient transportation of chain CM requires an exchange of partners between clusters. It has to be noted that this "hopping mechanism" has a different definition from the work of Rapp *et al.* [65], where "hopping" means the existence of a fully unassociated intermediate. We are here to distinguish it from the diffusion without involving associative reactions, which will be discussed in the following. We can now look back to the simplified expression for D_{cm}. Because the sticky friction δ can be replaced by τ_{sti}, D_{cm} will rely on the associative parameters in the form of $D_{cm} \sim (n_s \tau_{sti} \xi)^{-1}$. The product $n_s \tau_{sti}$ can be regarded as the overall hopping events required to diffuse for the length of a chain size. The association chemistry has shown that $n_s \tau_{sti}$ is nearly a constant, because the value of β in Eq. (18) is close to 2. As a result, the key factor in D_{cm} should be the background friction ξ, given a

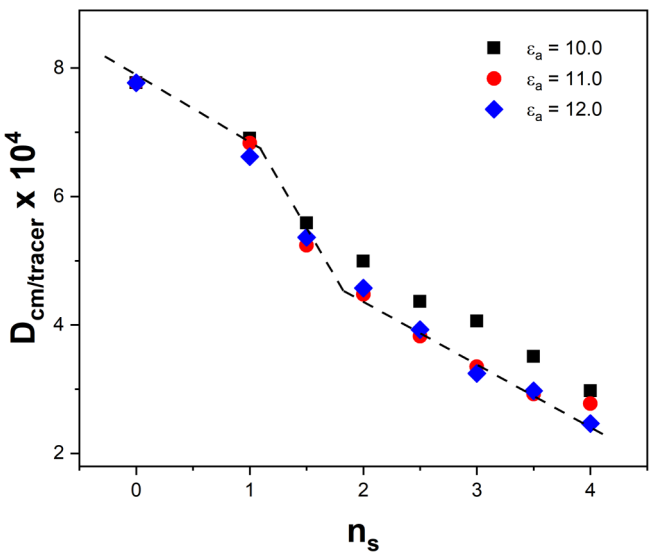

FIG. 7. CM diffusion constant of tracer chains $D_{cm/tracer}$ as a function of the number of stickers per chain n_s at different association energies. The dashed line is a guide for gelation transition.

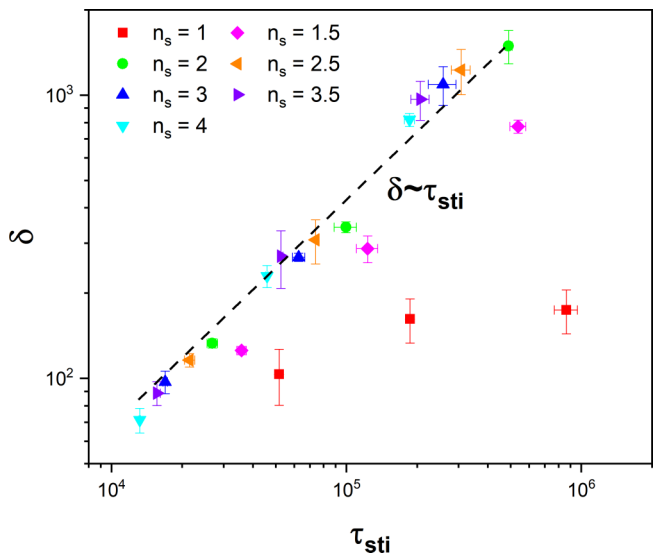

FIG. 8. Comparison between the relative frictional coefficient of stickers δ and the association relaxation time τ_{sti}. The dashed line denotes the linear relationship $\delta \sim \tau_{sti}$. Scatters of the same symbol stand for the same chain model with the association energy $\varepsilon_a = 10.0$, 11.0, and 12.0, respectively.

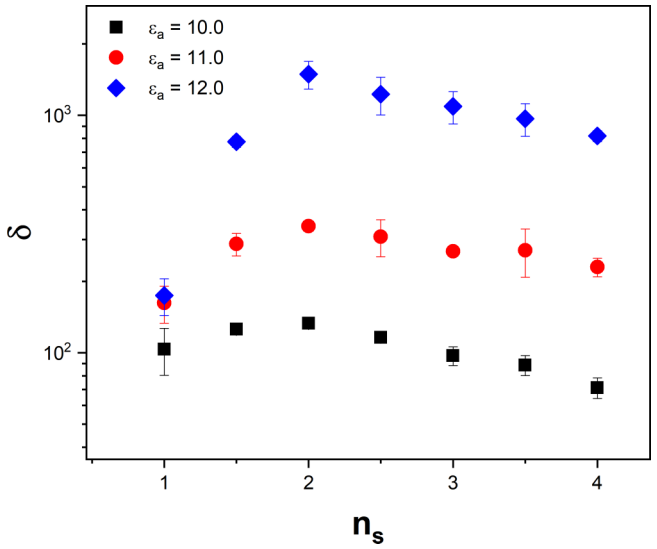

FIG. 9. Relative frictional coefficient of stickers δ as a function of the number of stickers per chain n_s.

fixed association energy. It is found in the simulation that the diffusibility is still penalized when new stickers are inserted, in spite of the acceleration of reactions. This phenomenon should be explained as the same number of hopping events happening in a more viscous background. With regard to experiments, it was reported by Colby *et al.* [66] that, in the sulfonated polystyrene (SPS) ionomer system, the diffusion constant follows $D_{cm} \sim n_s^{-2}$. According to our result, we should be very cautious when this scaling relationship can be directly applied. As long as the association chemistry is elaborately designed, D_{cm} may rely on n_s in a much indirect way.

As to the AP below gel point ($n_s = 1$), the growth of δ as a function of τ_{sti} is much smaller than that in the gel system. After considering the ungelated regime, the overall profile of δ in Fig. 9 is non-monotonic with the highest value at $n_s = 2$, below which the associative network is not fully developed. The reason for the limited value of δ in the SOL system is that the associative chains with $n_s = 1$ only form a star-like aggregate, and the single chain diffusion can be accomplished by either the hopping process or following the self-diffusion of chain aggregates, as has been pointed out in our previous work [23]. The latter mechanism relies on the aggregation number of stickers. Because the growth of aggregation numbers has been controlled by using the present simulation model with capped stickers, the self-diffusion process will always contribute a considerable part to the overall displacement. In contrast, the frequency of hopping will be gradually lowered with the increase in association energy. The contribution from hopping can be estimated quantitatively. Inputting the associative relaxation time τ_{sti} into the best-fit linear regression curve for the GEL systems (the dashed line in Fig. 8), we will know what the value of the sticky friction coefficient δ_0 should be if hopping is the only mechanism of diffusion. Also, the ratio δ/δ_0 can be regarded as the portion of hopping in the overall diffusion constant. In the case of $\varepsilon_a = 10.0$, 11.0, and 12.0, these ratios are approximately 40.8%, 22.9%, and 5.8%, respectively. These reveal that hopping gradually becomes a less important mechanism of diffusion. The discussion in this paragraph shows that the dynamics of associative chains and the associative reaction are not always coupled, while we are more likely to find a self-consistent description for associative systems from the concept of effective friction.

As a summary for this section, the relative frictional coefficient δ is extracted from the chain CM diffusion. After considering the change in the mean-field background friction, δ is found to be directly related to the association relaxation time τ_{sti} in the GEL regime, which strongly supports the basic assumption of the SRM that the relative retardation of stickers and the associative interaction can be mutually converted. However, their correlation can break down if the network structure has not fully developed. In the following sections, we will show how this Fick-diffusion property and the mechanical relaxation behavior are related by the SRM.

D. Linear viscoelasticity

The property with which we are concerned most is the viscoelasticity of APs and its relationship with molecular parameters. In the present equilibrium MD simulation, the linear relaxation modulus $G(t)$ is chosen to represent the bulk LVE property, which can be calculated from the time correlation functions of off-diagonal components of the stress tensor $\sigma_{\alpha\beta}$ based on the Green–Kubo relationship,

$$G(t) = \frac{V}{3k_BT}\left(\langle\sigma_{xy}(t)\sigma_{xy}(0)\rangle + \langle\sigma_{xz}(t)\sigma_{xz}(0)\rangle + \langle\sigma_{yz}(t)\sigma_{yz}(0)\rangle\right), \tag{21}$$

where the multi-tau correlator algorithm [67] is used to reduce the strong noise in the correlation functions. Also, the simulation time is chosen to be several orders of magnitude larger than the longest relaxation time. The simulation results for a different sticker number n_s and the association energy ε_a are shown in Figs. 10(a)–10(c). Clearly, the simulation results show regulation as expected. Compared with the homopolymer system, the profile of $G(t)$ in the SOL state is nearly undisturbed from association except for a slight hump in the terminal regime. Also, raising the association energy will not result in further differences, as shown in Fig. 10(b). By comparison, a distinctive plateau regime appears in all GEL polymers, which is exactly the characteristic of a network. Increasing the concentration of stickers will raise the height of the plateau regime, which is the case in Fig. 10(a), while its width or the rheological longest relaxation time τ_{max} is determined by the association energy, as shown in Fig. 10(c). It needs to be noticed that the elasticity of the network is not strictly coincident with the geometric connection state. For example, the $n_s = 3$ and $\varepsilon_a = 9.0$ systems are classified as a GEL, according to Fig. 3. However, it only shows very limited elasticity. This can be a unique property of a physical gel. The choice of connectivity or elasticity relies on the requirement in applications.

The dependence of the LVE function is highly consistent with the SRM calculation. In particular, these moduli can be directly predicted from the SRM, using the system parameters

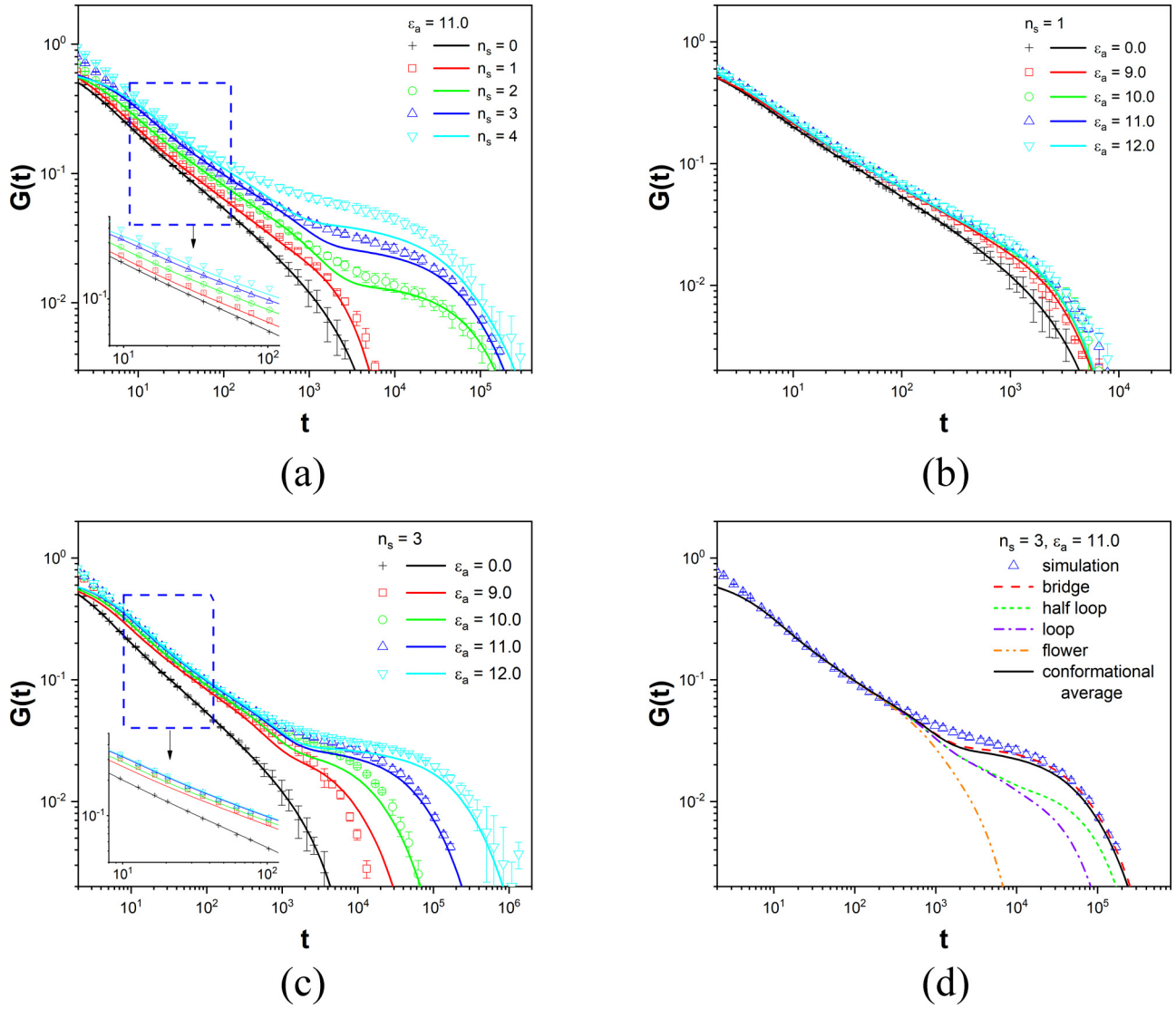

FIG. 10. Linear relaxation modulus $G(t)$ as a function of (a) n_s at $\varepsilon_a = 11.0$ and ε_a at (b) $n_s = 1$ and (c) $n_s = 3$. (d) The profiles of modulus predicted from different chain conformations. Scatters are from the simulation. The solid lines are the parameter-free predictions of SRM with conformational average. The values of δ are amplified by a factor of 3/2 compared with those defined from Eq. (20). The modulus for the rest of the parameters is presented in Fig. S7 [89].

and the quantities identified in the previous sections. For a specific conformation, the SRM predicts the linear relaxation modulus in the following form:

$$G(t) = \frac{\rho k_B T}{N} \sum_{p=1}^{N-1} \exp(-2t/\tau_p). \tag{22}$$

In the simulation system, the monomer density ρ, the reduced temperature $k_B T$, and the chain topologies are all predefined variables. The rest of the parameters in the full expression of $G(t)$ include the distribution functions of chain conformations, the relative frictional coefficient for stickers δ, and the unit of relaxation time, that is, $\tau_0 = \tau_p \lambda_p$. The conformational distribution functions have also been identified in Fig. 4, and the values of δ have been calculated from the diffusion constant. As to τ_0, according to its definition in Eq. (8) and the diffusion of tracer chains, τ_0 can also be expressed as $\tau_0 = b^2/3N_K D_{\text{cm/tracer}}$, where N_K is the Kuhn number. The Kuhn length b and the bond length l are related by $\langle \mathbf{R}_{ee}^2 \rangle = C_\infty N l^2 = N_K b^2$, where C_∞ is the characteristic ratio and is equal to 1.80 under the present simulation parameters. For the convenience of discussion, we regard each monomer as a Kuhn bead, that is, $N_K = N$. Finally, τ_0 will be calculated in the form of $\tau_0 = C_\infty l^2/3ND_{\text{cm/tracer}}$, where the equilibrium bond length is close to $l = 0.96$. Thus, this elementary timescale should be consistent with the tracer diffusion constant discussed in Fig. 7. As a result, it is possible to predict the LVE of APs from the SRM without any fitting parameters. Comparisons between the simulation results and the parameter-free predictions of SRM are shown in Fig. 10. A quantitative agreement is found in these profiles of modulus. For the homopolymer system, it is found that the simulation and theoretical result are almost perfectly matched, which shows that all the assumptions of the Rouse model are well satisfied in the simulation system, and all molecular parameters identified previously are in a reasonable range.

For the SOL polymer with $n_s = 1$ in Fig. 10(b), there is also a good agreement between the simulation and the SRM

prediction. The hump in the modulus relative to the homopolymer system is located exactly in the position predicted by the SRM. The change in the relaxation time spectrum τ_p represented by this hump is mainly attributed to the eigenvalues λ_p of the sticky RZ matrix, because the mean-field background friction in the SOL polymers is nearly unchanged compared with homopolymers, which means that τ_0 should also be an unchanged value. As for the GEL polymers, although not so perfect as the homopolymer and SOL polymer, considerable consistence is still found between the predicted curves and the simulation results. The Rouse regime, which appears before the elastic plateau and holds a $t^{-1/2}$ scaling dependence, is found to shift to a larger timescale compared with the homopolymer. Such a shift is sensitive to the density of crosslinking but is less affected by the strength of association, as shown in Figs. 10(a) and 10(c). According to the SRM, this Rouse regime contributes to the relaxation modes in the fast group. The eigenvalues corresponding to this group have only a limited response to the value of δ. Therefore, in contrast to the SOL polymer, the key factor that determines the relaxation times in this regime will be the elementary time τ_0. Also, the horizontal shift of this regime should be consistent with the tracer diffusion constant in Fig. 7. This prediction is exactly what we have observed in the simulation.

As to the plateau values of modulus G_N^0, the SRM predicts $G_N^0 = (\rho k_B T/N)(n_s - 1)$, which means that they are simply proportional to the number density of network strands. From Fig. 10(a), we can find that the heights of these plateau regimes in the simulation show a similar regulation. The theoretical values of G_N^0 are consistent with the affine network (AN) theory for rubber elasticity [55,68]. However, it is generally recognized that the elasticity of a real network should be described by the phantom network (PN) theory with the exclusion of topological defects [69]. The prediction from AN stands for the upper limit of elasticity. In this work, the effect of network defects has been considered. In Fig. 10(d), it is found that the network defects contributes only negligibly to elasticity. The prediction from bridge chains and the one with conformational average are nearly indistinguishable. With regard to the difference between AN and PN theory, the AN treats the network strand individually, while the PN allows the fluctuation of network junctions by regarding the whole network as a single giant molecule [55]. An associative network should be treated as the collection of individual chains, as has been indicated by the SRM, so it is closer to the description of an AN. In addition, the present simulation system will probably not distinguish PN from AN even if the association energy is raised to infinity. Because the junctions in the simulation systems are clusters and crowded with cap monomers, they have a hindered mobility compared with those in a classic chemical network. As a result, the difference between AN and PN theory shall be erased to some extent. From the other point of view, the relaxation time spectrum of the simulation system is more continuous than the theoretical prediction of SRM, and the plateau value in the $n_s = 4$ system is even higher than the upper limited given by the AN theory. These facts suggest that the expression of stress in Eq. (1) may be too ideal for the simulation system. One possible cause is the structure of junctions. Although the number of stickers that aggregate in a single cluster is limited, the transient junction is still crowded with cap monomers, which increases the local concentration of monomers and brings perturbation to Eq. (1).

When it comes to the terminal regimes of modulus determined by the sticky friction, it is found using the values of δ obtained from Eq. (20) will underestimate the terminal relaxation time τ_{max}. However, by simply amplifying δ by a factor of 3/2, the predicted terminal regimes will be overlapped with the simulation within statistic errors. Considering that the theoretical foundation of the SRM is the ideal expression of stress in Eq. (1), which is derived by assuming that the Gaussian spring potential is the only interaction of the polymer system, this constant amplification factor in δ is totally acceptable. Moreover, the stress-optical law allows the existence of a constant factor that is independent of the molecular structures on the large length scale [17]. To this extent, we can still say that the theoretical prediction of the SRM quantitatively agrees with the simulation result in a parameter-free style. Also, the diffusion properties of the associative chains and the bulk LVE mutually agree with each other and are well connected by the SRM. The other phenomenon that needs to be noticed is the change in τ_{max} as a function of n_s, which is presented in Fig. 10(a). With a higher value of n_s, only a limited expansion of the terminal time is observed and the plateau regime experiences an earlier decay. The dependence of τ_{max} can be understood from the relationship $\tau_{max} \approx \left\langle R_g^2 \right\rangle / D_{cm}$. Now that the overall chain size is nearly fixed, τ_{max} will show a very similar regulation with D_{cm}. As has been discussed previously, the most considerable contribution comes from the background friction ξ. Another factor that matters in the modulus profiles is the structure defect. According to Fig. 4, inserting new stickers or shortening the strand between neighboring stickers will bring more intra-chain associations. Evidently, these defects will contract the terminal regime, as shown in Fig. 10(d).

It also needs to be explained how to relate this limited growth of terminal time observed in the simulation to experimental systems. Experimentally, it is usually found that raising the sticky motifs will significantly expand the terminal regimes [6,48]. In the present work, the limited expansion can be easily explained from the association chemistry simulated by the capped chain model, which allows an acceleration of reactions by introducing additional reactants. However, such an association chemistry is not realized in many experimental systems. For example, in hydrogen bonding systems, stickers like acrylic acid (AA) and ureido-pyrimidinone (Upy) will form not only a binary assembly but also a collective assembly [48,70,71]. Raising the content of the sticky components will probably enlarge the junction size and the association activation energy. In ionomer polymers like SPS neutralized with alkali counterions, although the high dielectric multiplets have a fixed size, the chain segments still suffer more restriction in mobility at a higher ion content according to the model proposed by Eisenberg and Moore [36], which can lead to a hindered reaction chemistry. In order to observe the limited

growth in τ_{max} experimentally, the best choice is to refer to a metallo-associating system, where the chemical structure of the junctions can be fixed. In fact, some clues that support this argument can be found in the experimental work by van Ruymbeke and co-workers [50]. Another factor that influences the judging of the terminal regime is the time-temperature superposition principle (tTSP), which is not applied in the present simulation but is widely observed to have failed in APs [13,72,73]. Although in most cases a rheological master curve can always be obtained, fitting those shifting coefficients via the Williams–Landel–Ferry (WLF) function may require multiple groups of parameters [74]. Two factors are thought to be the causes of failure [75]. One is related to a change of chemical structures. The other is the restricted motion caused by association, with the motion of the precursor segment probably having different responses to the temperature. The terminal time obtained from tTSP can be examined from the dielectric response in some cases [7]. Its connection and difference from viscoelastic relaxation in APs can be understood from the theory developed by Watanabe *et al.* [76,77].

E. Segmental diffusion and internal relaxation

The most attractive part of the SRM is that it reveals the connection between LVE and the motion of segments. The characteristic time and length scales of APs can also be found in the internal relaxation of segments, which will provide significant supplement to the LVE property. In particular, these diffusive behaviors can also be directly predicted by the SRM. In order to do this, we need the exact form of normal transformation. It is found that the pth normal coordinate can be approximately expressed as

$$\mathbf{X}_p \approx \sqrt{N}\sum_{i=1}^{N} \mathbf{r}_i \xi_i \cos\left[\frac{p\pi}{N}\left(i-\frac{1}{2}\right)\right] \Big/ \sum_{i=1}^{N} \xi_i. \tag{23}$$

Compared with the classic Rouse mode expression, the contribution of a segment to the normal coordinate is weighted by its effective friction in the SRM. From the zeroth normal coordinate, we can identify a so-called effective center-of-mass, that is,

$$\mathbf{r}_{\mathrm{cm/eff}} = \nu_i^0 \mathbf{X}_0 = \sum_{i=1}^{N} \xi_i \mathbf{r}_i / \sum_{i=1}^{N} \xi_i. \tag{24}$$

In a homopolymer, $\mathbf{r}_{\mathrm{cm/eff}}$ is exactly the chain CM $\mathbf{r}_{\mathrm{cm}}$, while in the AP, $\mathbf{r}_{\mathrm{cm/eff}}$ moves to the center of the stickers when $\delta \gg 1$. For the chain models discussed in the previous sections, because the stickers are uniformly distributed, there will be no significant difference between $\mathbf{r}_{\mathrm{cm}}$ and $\mathbf{r}_{\mathrm{cm/eff}}$. However, if the distribution of stickers is in a non-symmetric fashion, like blocky or gradient, the two kinds of definition of the chain center will be much more distinguishable. Based on this definition, the inverse form of the normal transformation in Eq. (9) can be rewritten as

$$\mathbf{r}_i = \mathbf{r}_{\mathrm{cm/eff}} + \sum_{p=1}^{N-1} \nu_i^p \mathbf{X}_p. \tag{25}$$

Then, we will have the overall MSD of the ith segment,

$$\begin{aligned} g_1^i(t) &= \left\langle [\mathbf{r}_i(t) - \mathbf{r}_i(0)]^2 \right\rangle \\ &= \left\langle \left\{ [\mathbf{r}_{\mathrm{cm/eff}}(t) - \mathbf{r}_{\mathrm{cm/eff}}(0)] + \sum_{p=1}^{N-1} \nu_i^p [\mathbf{X}_p(t) - \mathbf{X}_p(0)] \right\}^2 \right\rangle \\ &= \left\langle [\mathbf{r}_{\mathrm{cm/eff}}(t) - \mathbf{r}_{\mathrm{cm/eff}}(0)]^2 \right\rangle + 2\sum_{p=1}^{N-1} (\nu_i^p)^2 \left[\left\langle \mathbf{X}_p(t) \cdot \mathbf{X}_p(t) \right\rangle - \left\langle \mathbf{X}_p(t) \cdot \mathbf{X}_p(0) \right\rangle \right] \\ &= \left\langle [\mathbf{r}_{\mathrm{cm/eff}}(t) - \mathbf{r}_{\mathrm{cm/eff}}(0)]^2 \right\rangle + \frac{6}{\xi^2} \sum_{p=1}^{N-1} \tau_p \left\langle f_{p\alpha}^2 \right\rangle (\nu_i^p)^2 [1 - \exp(-t/\tau_p)]. \end{aligned} \tag{26}$$

To focus on the relaxation behavior, the MSD of a segment relative to the effective center $g_2^i(t)$ is recommended, which is defined as

$$\begin{aligned} g_2^i(t) &= \left\langle \{ [\mathbf{r}_i(t) - \mathbf{r}_{\mathrm{cm/eff}}(t)] - [\mathbf{r}_i(0) - \mathbf{r}_{\mathrm{cm/eff}}(0)] \}^2 \right\rangle \\ &= \frac{6}{\xi^2} \sum_{p=1}^{N-1} \tau_p \left\langle f_{p\alpha}^2 \right\rangle (\nu_i^p)^2 [1 - \exp(-t/\tau_p)]. \end{aligned} \tag{27}$$

Apparently, the mechanical and segmental relaxation will share the same relaxation modes, but the relaxation times in the LVE functions should be only half the segmental relaxation time, which is indicated by the normalized form of stress in Eq. (10). In the classic Rouse model, $g_2^i(t)$ has the following analytical form:

$$g_2^i(t)_{(\mathrm{Rouse})} = \frac{6k_{\mathrm{B}}T}{\xi N^2} \sum_{p=1}^{N-1} \tau_p \cos^2\left(\frac{p\pi i}{N}\right) [1 - \exp(-t/\tau_p)]. \tag{28}$$

Here, we preserve the form of relaxation times to emphasize the change in eigenvectors. From the existing literature

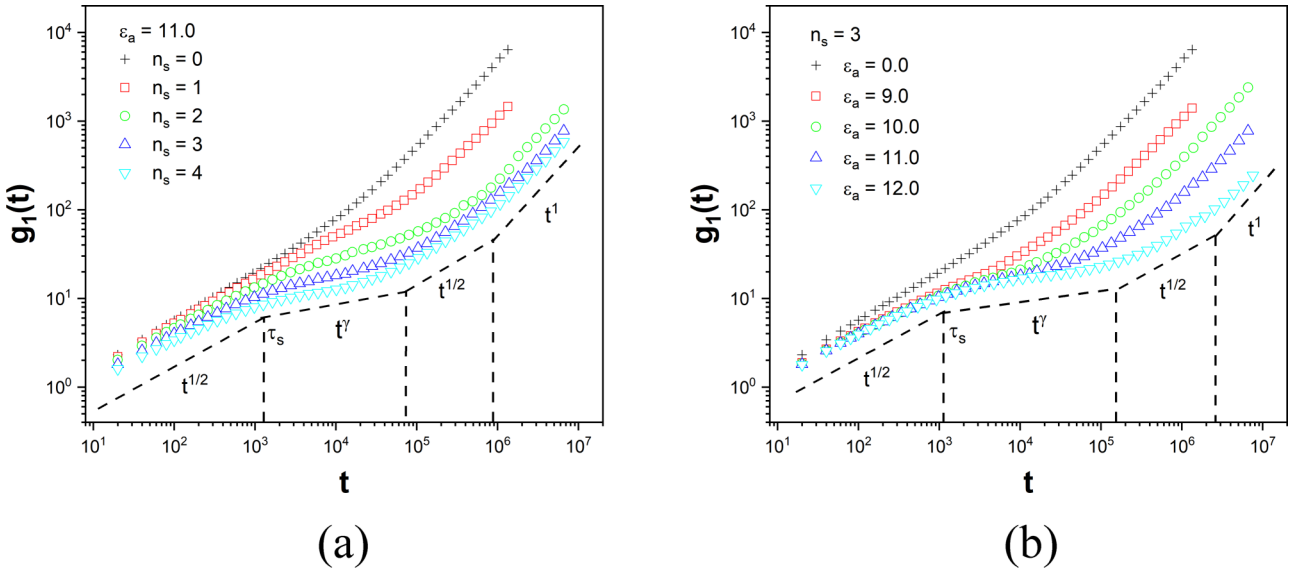

FIG. 11. The mean values of overall segmental MSD $g_1(t)$ as a function of (a) the number of stickers per chain n_s and (b) association energy ε_a. The scaling exponent $\gamma = 1/6$ in (a) but $\gamma = 1/8$ in (b).

studies, it is found that the Rouse model with frictional heterogeneity has been applied to investigate the suppressed segmental dynamics in the ion-doped polymers [78]. Here, a more meticulous discussion will be presented, which sticks to the physical picture of the SRM. From the simulation perspective, it is straightforward to get the profiles of a segmental MSD. With the knowledge of δ, it is easy to locate the effective center. Also, a theoretical curve will only require the values of δ, the time unit τ_0, and the conformational distribution functions, which are all known quantities as discussed in the previous section. So, the following comparison between the simulation results and the theoretical prediction is also free of adjustable parameters.

The mean values of the overall MSD $g_1(t)(=\sum_{i=1}^{N} g_1^i(t)/N)$ and the relative MSD $g_2(t)(=\sum_{i=1}^{N} g_2^i(t)/N)$ as a function of the sticky content and association energy are shown in Figs. 11 and 12, respectively. The scaling behavior in these segmental diffusion functions is quite noticeable. As expected, in the absence of associative interaction, a single scaling transition from $t^{1/2}$ to t^1 is observed in $g_1(t)$ (another regime with t^1 scaling below the length scale of a Kuhn length is not shown here). The former regime means that the segmental motion is constrained by connectivity, while the latter (the Fick regime) means that the internal structure has been fully relaxed and a segment is subjected to the CM diffusion. The SOL polymer with $n_s = 1$ shows a very similar scaling feature as

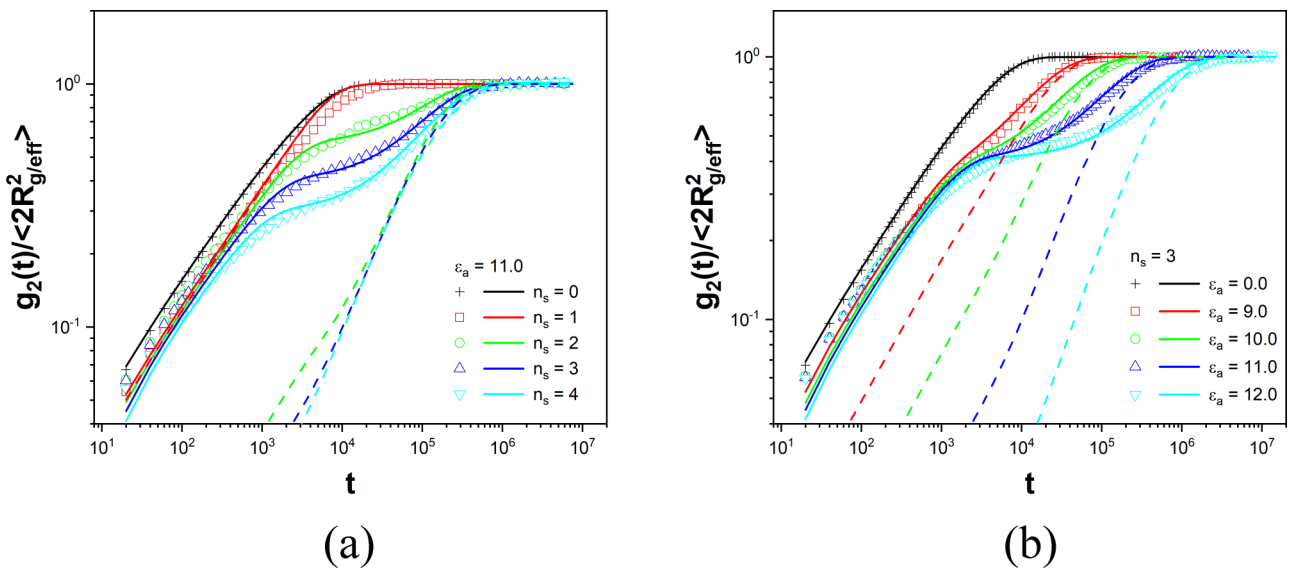

FIG. 12. The mean values of a segmental MSD relative to the effective CM divided by chain size $g_2(t)/\left\langle 2\mathbf{R}^2_{g/eff}\right\rangle$ as a function of (a) the number of stickers per chain n_s and (b) association energy ε_a. Scatters are the results from simulation. The solid lines are the parameter-free prediction from the SRM with conformational average. The dashed lines denote the theoretical curves when the relaxation times are substituted into Eq. (28). The diffusion functions for the rest of the parameters are presented in Fig. S8 [89].

the homopolymer, but the transition to the Fick regime is delayed, which means a slowdown of diffusion caused by associative interaction, as shown in Fig. 11(a). However, in the GEL polymers, like the appearance of a plateau regime in the linear relaxation modulus $G(t)$, a new transition regime with a scaling dependence t^{γ} is observed in $g_1(t)$ after a characteristic time τ_s, followed by another $t^{1/2}$ regime before the Fick diffusion. The value of the scaling exponent γ is much smaller than 1/2, so this transition regime means a more retarded motion in a percolated network. From Fig. 11, it should also be noticed that γ is nearly identical in the GEL polymers with different contents of stickers, but is strongly influenced by the association energy. With the increase in association strength, this regime is not only broadened, but also flattened, and will finally turn to a plateau in the case of permanent association. The corresponding length scale of this transition regime is the network strand, that is, $g_1(\tau_s) = \left\langle 2\mathbf{R}_g^2(\bar{N}_s)\right\rangle$, and the regime before τ_s stands for the less affected motions inside the network strand. Apparently, it will be easier for the monomers to feel the constraint of stickers when the network is more densely crosslinked, which suggests an earlier appearance of this transition regime. The overall division of scaling regimes in $g_1(t)$ is very similar to that in a well entangled homopolymer system. According to the classic tube model [17], τ_s can be analogous to the entanglement time from which the segments start to feel the constraint of the tube, and the start of the Fick regime is the disentanglement time after which no segment survives in its original tube. Compared with the experiments by Olsen and co-workers [22], the super-diffusion with a time scaling exponent larger than one is not found in the present work, which indicates the existence of other mechanisms rather than sticky Rouse dynamics in their systems.

The comparison between the theoretical prediction of the SRM and the simulation is shown in the profiles of $g_2(t)$ in Fig. 12. The values of δ defined from Eq. (20) are directly adopted for the theoretical curves, because both the CM diffusion and segmental diffusion belong to single chain dynamics and the expression of stress is not involved. The dashed lines in Fig. 12 stand for the theoretical curves when the relaxation times are substituted into Eq. (28). They will show the behaviors when the sticky Rouse relaxation time spectrum follows the classic Rouse relaxation modes. According to the definition of $g_2(t)$ in Eq. (27), $g_2(t)$ will end with a plateau regime in the long time limit, that is, $g_2(t \gg \tau_{max}) = \left\langle 2\sum_{i=1}^{N}(\mathbf{r}_i - \mathbf{r}_{cm/eff})^2\right\rangle/N \equiv \left\langle 2\mathbf{R}_{g/eff}^2\right\rangle$, where $\left\langle \mathbf{R}_{g/eff}^2\right\rangle$ is defined as the effective radius of gyration. So, the simulation results for $g_2(t)$ are rescaled by this effective chain size. In the profiles of $g_2(t)$, the feature of the transition scaling regime in the associative network is more pronounced, and the characteristic times, including τ_s and τ_{max}, are easier to identify. From Fig. 12, it is surprising to find that the features observed in $g_2(t)$ are all successfully predicted by the SRM. Also, the changes in eigenmodes, including the eigenvalues and eigenvectors, are both non-trivial factors, because the dashed lines in Fig. 12 fail to predict the simulation results. For the homopolymer system, like the case in Fig. 10 for modulus, the segmental diffusion function also perfectly matches the theoretical prediction. This means that in the present simulation box where the polymers suffer pure repulsive interaction and FENE bond interaction, the single chain dynamics are closely related to the viscoelastic behavior. Thus, the expression of stress in Eq. (1) can be applied without any modification.

As for the polymers with stickers, the agreement between theory and simulation is still considerable. Also, it can be concluded that the segments in a melt of AP indeed suffer a similar constraint as a free-draining chain under inhomogeneous friction. For $g_2(t)$ in the SOL polymer with $n_s = 1$, the scaling behavior before the terminal time is found to be changed from the $t^{1/2}$ relationship predicted by the classic Rouse model. By comparison, such a change is not so obvious in $g_1(t)$. Therefore, we suggest that $g_2(t)$ should be a more appropriate function for segmental relaxation. In the GEL polymers, the characteristic transition regime is also captured by the SRM. Also, the theoretical variation as a function of the sticky content and association energy is consistent with the simulation results. In addition, we can reach a much more quantitative agreement between theory and simulation than the moduli in Fig. 10, especially after the contribution from each conformation is considered. In Fig. 13 for the $n_s = 3$ and $\varepsilon_a = 11.0$ systems, it can be seen that the simulation result is exactly located in between the predictions from a bridge chain and a half loop chain, which are the two dominant conformations, as has been discussed previously. It is proved in some period of time that the segments relax in a chain model with a ring topology. From the agreement in $g_2(t)$, we can say that it is completely possible to track the exact Brownian motion of a single associative chain from the SRM. Even so, there is a gap in predicting the rheological properties mainly due to the microscopic expression of stress. But in some associative systems and for some properties that

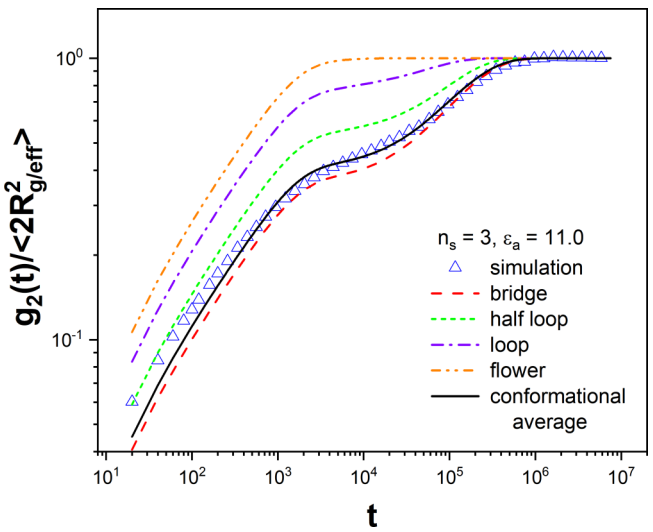

FIG. 13. Segmental diffusion function $g_2(t)/\left\langle 2\mathbf{R}_{g/eff}^2\right\rangle$ of different chain conformations at $n_s = 3$ and $\varepsilon_a = 11.0$, and their comparison with the simulation result. The effect of conformation in other chain models is shown in Fig. S9 [89].

we are mostly concerned about, this gap can be amended by simply introducing a constant value to the oversimplified form for stress.

The profiles of $g_2^i(t)$ differ significantly according to the positions of segments in the chain, and the prediction of the SRM is considerably reliable even in such an individual level, as shown in Fig. 14. Usually, the outer monomers have higher mobility than the inner ones with a larger terminal value of $g_2^i(t)$, because they are more distant from the chain CM. But in the presence of association, the mobility of a monomer will be determined by its distance from stickers, because the effective center $\mathbf{r}_{\mathrm{cm/eff}}$ is mainly determined by the position of the stickers according to its definition in Eq. (24). Also, from the relaxation of individual segments, it is found that the effective center is a nontrivial definition even in a symmetric chain. A detailed discussion is presented in Sec. S6 of the supplementary material [89]. For the homopolymer in Fig. 14(a), it can be seen that not only $g_2(t)$, but also the values of $g_2^i(t)$ for any chain segment are precisely predicted by the classic Rouse model. So, a melt-state bead–spring chain with hard-sphere repulsion indeed follows the equation of motion described by the Rouse model, even though the basic formulation ignores all conservative interactions except for a Gaussian spring potential. When there is one sticker in the middle of the chain, which is the case in Fig. 14(b), few changes can be observed in the outermost monomer. However, there is an apparent slowdown when a monomer approaches the chain center, which shows the constraint of association, and this is consistent with the SRM prediction. Nevertheless, a noticeable discrepancy between theory and simulation is still found, especially when the monomer is adjacent to the sticker. The conformational effect is not the reason for this discrepancy, because there is only one kind of conformation in the case of $n_s = 1$. The discrepancy may arise from the nature of a sticker. Because a sticker in the simulation system is aggregated inside a cluster and crowded with cap monomers, the actually Kuhn size of the sticker should be larger than that of a non-sticky monomer. However, the SRM is formulated by assuming that a sticker and a normal bead differ only in terms of their frictions. This explanation

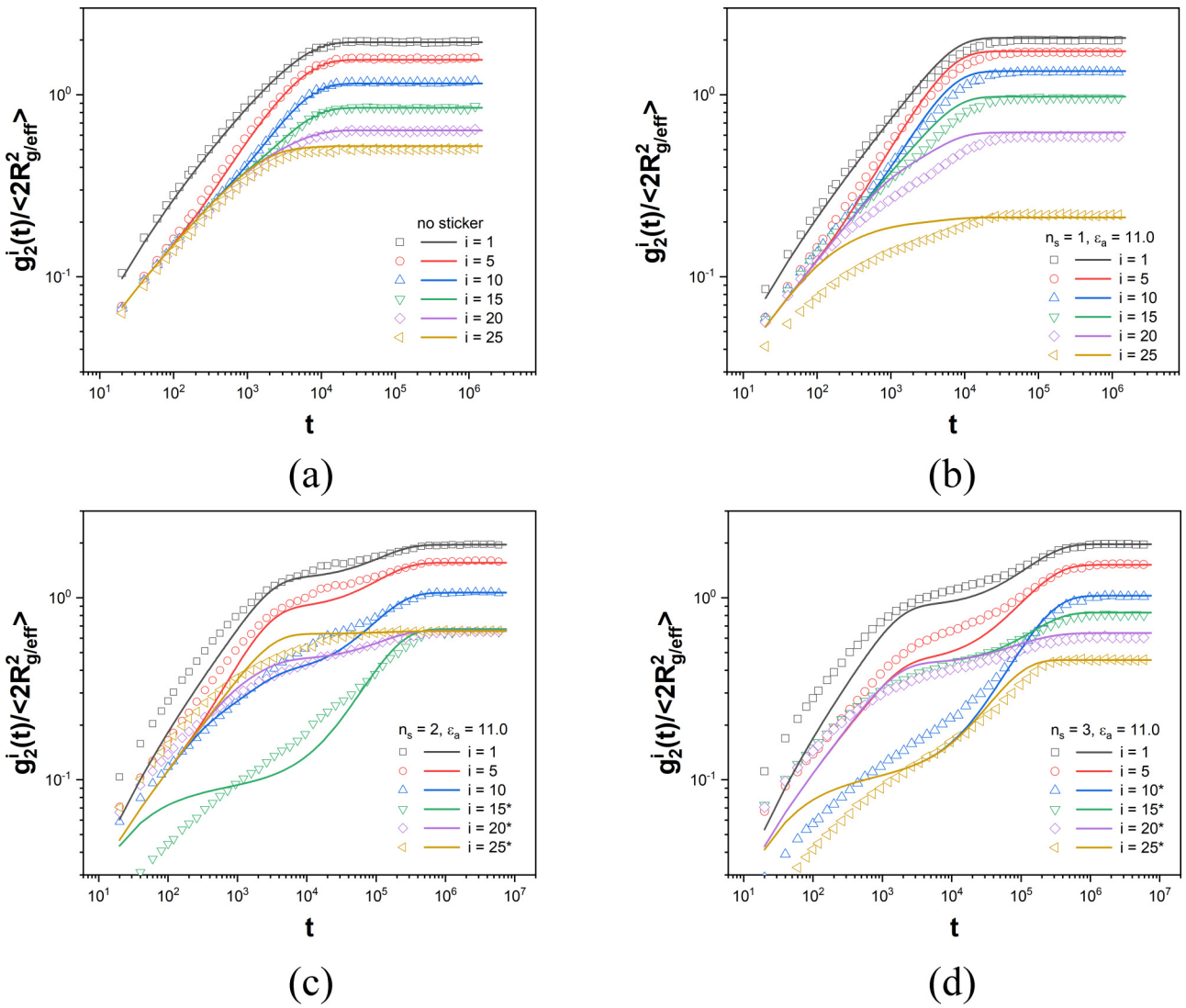

FIG. 14. Relative MSD of an individual segment $g_2^i(t)$. (a)–(d) stands for chain models with sticker number $n_s = 0, 1, 2, 3$, respectively. The outer most segment is labeled as $i = 1$. The star notation represents the segment in the interior of the network strand. The solid lines are the prediction of the SRM from the bridge conformation.

should also be applied to other associative systems. When there are multiple stickers in APs, the theoretical prediction still shows a very similar regulation with the simulation results. Particularly, the characteristic times are shared by the motion of each bead, which is consistent with the prediction of Eq. (27).

The connection between LVE and segmental diffusion is a universal property that raises from the expression of stress in Eq. (1) and should be found in any system. In particular, the above characteristics of APs are very similar to those in a well entangled homopolymer system. The modulus profile of an entangled polymer is also characterized by a plateau regime, demonstrating that an entangled system has the nature of a transient network and shares a similar relaxation time spectrum with APs. In the segmental diffusion property, the appearance of a $t^{1/4}$ scaling regime in the overall MSD of the chain segment is another symbol of the entanglement effect, which is very similar to the transition regime of the AP in Fig. 11. From the physical picture in Fig. 1, it is easy to understand why an AP system and a well entangled homopolymer system will display similar behavior at the molecular level, by assuming that the reactive site in Fig. 1(a) is analogous to an entanglement site and that it acts only on some specific segments. As a result, we can expect a sticky Rouse description for entanglement effect. In particular, if the entanglement effect is allowed to act on any segment, that is, if the positions of stickers are totally random, we can find a very similar regulation like the effect of contour length fluctuation, which is discussed in Sec. S7 [89]. In fact, the reasoning that the entanglement effect can be understood from a modified Rouse model can be traced back to the work of Chompff *et al.* [79,80] and later reconstructed by Hong *et al.* [81]. In Hong's work [81], the Rouse model with inhomogeneous friction was used and the entanglement effect was included in the effective friction of a sticky segment. By treating δ as a power law function of the entanglement length, a good agreement was found between the theoretical modeling and the experimental measurement of LVE functions. Except for relaxation behavior, other similarities between APs and entangled polymers have also been pointed out by Weiss and co-workers [73,82,83], and one example of such similarity is flow activation energy. In spite of these similarities, it still needs to be noted that the two types of interaction are different in nature. Entanglement is defined by a single parameter, i.e., the entanglement length, while an AP is characterized by the number of stickers and the strength of association. Their difference is more pronounced when it comes to the nonlinear viscoelastic properties. Some characteristic behaviors of an entangled system, like stress overshoot upon start-up flow, are not always observed in associative systems, for example, the SPS melt [82]. In the same kind of an AP, the scaling dependence of shear viscosity or first normal stress coefficient on the shear rate is also different from that in entangled polymers [83]. The reason for these differences is thought to be the brittleness of the elastic-determining ionic nanodomains in SPS. Despite these observations, it is still worthwhile to complete the physical picture for entanglement under the sticky Rouse description.

F. Chain model with asymmetrically distributed stickers

It has been expected the SRM discussed in the present work can be applied to any molecular structure. To prove this, chain models with asymmetrically distributed stickers are built. In the asymmetric AP chain with $n_s = 2$, the two stickers are repositioned to 1 and $N/2$, respectively, in contrast to $N/4$ and $3N/4$ in the symmetric case. By fixing the length of a network strand, the network structures and the conformational distribution functions are expected to be unchanged. Thus, the effective frictions for both the sticky and non-sticky segments will be identical to those in a symmetric AP. In this way, we can focus on how the relaxation modes are changed when only the effective CM is moved to a biased position.

A comparison of the linear relaxation modulus $G(t)$ and the segmental relaxation functions $g_2(t)$ between a symmetric and an asymmetric AP is shown in Fig. 15. The theoretical curves for the symmetric and asymmetric APs differ only in the frictional matrix $\boldsymbol{\Xi}$ that describes the positions of stickers. The rest of the parameters are all set to be identical because, as expected, the CM diffusion constant D_{cm}, the tracer chain diffusion constant $D_{cm/tracer}$, and the association relaxation time τ_{sti} are all found to be unchanged. It is clear from the simulated modulus in Fig. 15 that, although the chain topology is only slightly manipulated, there is indeed a change in the distribution of relaxation times. The symmetric AP has a larger terminal relaxation time than the asymmetric AP, while in the intermediate timescale, the modulus in the asymmetric AP is higher than that in the symmetric AP. So, in the asymmetric AP, the transition from the fast modes to slow modes is not so sharp due to the presence of a long dangling tail. Such a change in the relaxation spectrum is correctly predicted by the SRM. It is proved that the SRM is still applicable after altering the positions of the stickers, making it a much more generalized model in describing the LVE of APs. The difference between symmetric and asymmetric APs and the consistence between simulation results and SRM theoretical prediction are also found in the segmental diffusion function, so the connection between LVE and segmental diffusion predicted by the SRM is always valid. Except for this, it needs to be noted that the effective chain size $\left\langle \mathbf{R}^2_{g/eff} \right\rangle$ is increased from 16.63 to 26.87 after the stickers are moved from the symmetric to the asymmetric case, so the two profiles of $g_2(t)/\left\langle 2\mathbf{R}^2_{g/eff} \right\rangle$ in Fig. 15 do not overlap in the Rouse regime.

The result in the present section not only further proves the validity of the SRM, but also indicates that the LVE properties of APs can be decoupled from the associative interaction by altering the positions of stickers. In some experimental works, the distribution of stickers has been found to be an important parameter [84–87]. For example, by crowding the stickers to outer regimes, the longest relaxation time will be expanded in the PnBA-Upy associative system [84]. In a perspective paper by Golkaram and Loos [88], the influence of a sticker's position is also discussed. The specific cases where the stickers are hinged as a backbone, side group, or other architectures are illustrated, respectively. Under the framework of the SRM, the

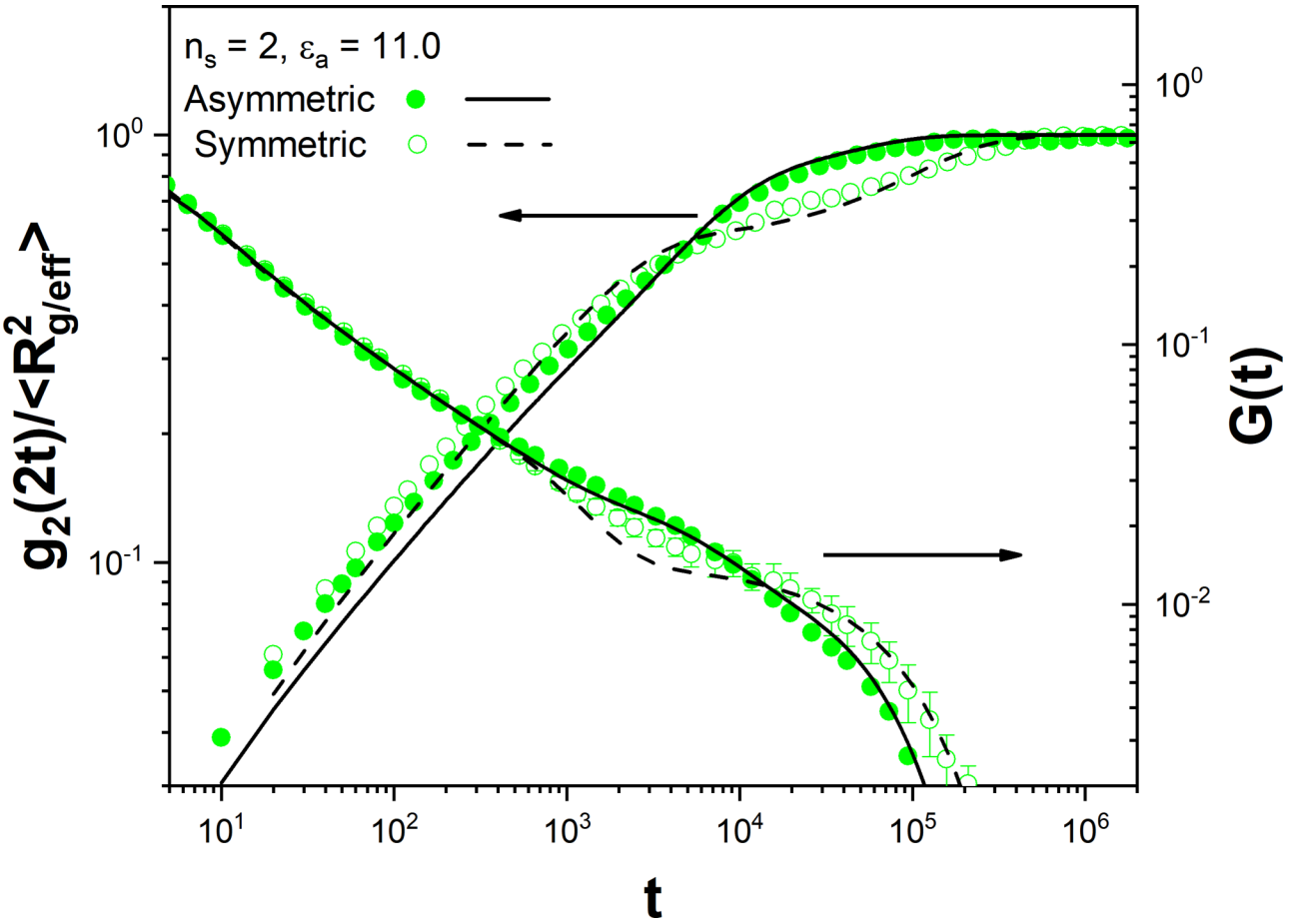

FIG. 15. Comparison of linear relaxation modulus $G(t)$ and segmental MSD relative to the effective chain CM $g_2(t)/\left\langle 2\mathbf{R}^2_{g/eff}\right\rangle$ between a symmetric and an asymmetric AP.

molecular origin of these strategies can be easily understood, that is, the same amplitude of associative interaction can affect the single-chain Brownian motion in different ways. This knowledge will help in the design of molecular structures that promise the most favored properties.

V. CONCLUSION

In summary, extensive MD simulations were carried out to check the idea of SRM, which has provided an indirect picture to understand the linear rheology of unentangled AP. Considering the theoretical foundation of the SRM, a simulation model with capped stickers was proposed to control the aggregation of stickers. From the CM diffusion of both the component and tracer chains, the relative sticky frictional coefficient, which is thought to be the key parameter in the SRM, was obtained and found to be consistent with the dynamics of associative reactions. Based on this, a linear relaxation modulus was predicted without involving fitting parameters. A quantitative agreement between theory and simulation was found, which shows the effectiveness of the SRM in predicting the LVE behaviors of APs. As a supplement to LVE, the segmental diffusive properties, including the overall diffusion and the diffusion relative to the effective chain center, were investigated. The former function was found to show a similar scaling behavior as a well entangled homopolymer, which further suggested the connection between associative interaction and the entanglement effect at the molecular level. Also, the latter function was also predicted by the SRM in a parameter-free style, showing that the dragging effect caused by associative interaction indeed can be understood as the local increase of friction on stickers. In particular, it was proved that the SRM could predict the dynamics of a single associative chain with considerable accuracy. Finally, the SRM was successfully applied to the associative system with asymmetric chains. From the results of this work, it is strongly believed that the SRM can serve as a molecular model for the dynamics of APs and that it has the power to connect properties at different molecular levels.

Except for the agreement with the sticky Rouse mechanism, the present work also suggests that the dynamics in a real associative system can be influenced by certain other factors, including the microscopic expression of stress, the effect of intra-chain association, the detailed association chemistry, and the definition of stickers. In particular, more attention needs to be paid to the expression of stress or the validity of the stress-optical law in APs, because it will directly support the single chain approach to model the rheology of APs.

From the simulation perspective, the scope of the present work can be further extended by exploring more sophisticated

situations, such as more complicated chain topologies, different concentration regimes, and systems with microphase separation, or by applying different simulation methods. It is worthwhile to check to what extent the SRM description for an unentangled AP remains valid. From the theoretical perspective, it can also be a good prospect to apply the concepts of the SRM to APs in an entangled regime, which will probably give a clearer molecular picture on the interplay between the entanglement effect and associative interactions.

ACKNOWLEDGMENTS

The authors are grateful to the valuable comments from all reviewers. The authors also thank the National Natural Science Foundation of China (NNSFC) (Grant Nos. 21774027, 21973017, and 21534002) for financial support.

REFERENCES

[1] Dzhardimatieva, G. I., B. C. Yadav, S. Singh, and I. E. Uflyand, "Self-healing and shape memory metallopolymers: State-of-the-art and future perspectives," Dalton Trans. **49**, 3042–3087 (2020).

[2] Perera, M. M., and N. Ayres, "Dynamic covalent bonds in self-healing, shape memory, and controllable stiffness hydrogels," Polym. Chem. **11**, 1410–1423 (2020).

[3] Lu, W., X. Le, J. Zhang, Y. Huang, and T. Chen, "Supramolecular shape memory hydrogels: A new bridge between stimuli-responsive polymers and supramolecular chemistry," Chem. Soc. Rev. **46**, 1284–1294 (2017).

[4] Seiffert, S., and J. Sprakel, "Physical chemistry of supramolecular polymer networks," Chem. Soc. Rev. **41**, 909–930 (2012).

[5] Van Ruymbeke, E., "Preface: Special issue on associating polymers," J. Rheol. **61**, 1099–1102 (2017).

[6] Zhang, Z. J., Q. Chen, and R. H. Colby, "Dynamics of associative polymers," Soft Matter **14**, 2961–2977 (2018).

[7] Chen, Q., G. J. Tudryn, and R. H. Colby, "Ionomer dynamics and the sticky Rouse model," J. Rheol. **57**, 1441–1462 (2013).

[8] Rubinstein, M., and A. N. Semenov, "Thermoreversible gelation in solutions of associating polymers. 2. Linear dynamics," Macromolecules **31**, 1386–1397 (1998).

[9] Leibler, L., M. Rubinstein, and R. H. Colby, "Dynamics of reversible networks," Macromolecules **24**, 4701–4707 (1991).

[10] Rubinstein, M., and A. N. Semenov, "Dynamics of entangled solutions of associating polymers," Macromolecules **34**, 1058–1068 (2001).

[11] Cates, M. E., "Reptation of living polymers: Dynamics of entangled polymers in the presence of reversible chain-scission reactions," Macromolecules **20**, 2289–2296 (1987).

[12] Baxandall, L. G., "Dynamics of reversibly crosslinked chains," Macromolecules **22**, 1982–1988 (1989).

[13] Chen, Q., C. Huang, R. A. Weiss, and R. H. Colby, "Viscoelasticity of reversible gelation for ionomers," Macromolecules **48**, 1221–1230 (2015).

[14] Jongschaap, R. J. J., R. H. W. Wientjes, M. H. G. Duits, and J. Mellema, "A generalized transient network model for associative polymer networks," Macromolecules **34**, 1031–1038 (2001).

[15] Wientjes, R. H. W., R. J. J. Jongschaap, M. H. G. Duits, and J. Mellema, "A new transient network model for associative polymer networks," J. Rheol. **43**, 375–391 (1999).

[16] Indei, T., and J. Takimoto, "Linear viscoelastic properties of transient networks formed by associating polymers with multiple stickers," J. Chem. Phys. **133**, 194902 (2010).

[17] Doi, M., and S. F. Edwards, *The Theory of Polymer Dynamics* (Oxford University, New York, 1986).

[18] Watanabe, H., "Slow dynamics in homopolymer liquids," Polym. J. **41**, 929–950 (2009).

[19] Yang, Y. L., "Graph theory of viscoelastic and configurational properties of Gaussian chains," Macromol. Theory Simul. **7**, 521–549 (1998).

[20] Rao, A., H. Yao, and B. D. Olsen, "Bridging dynamic regimes of segmental relaxation and center-of-mass diffusion in associative protein hydrogels," Phys. Rev. Res. **2**, 043369 (2020).

[21] Ramirez, J., T. J. Dursch, and B. D. Olsen, "A molecular explanation for anomalous diffusion in supramolecular polymer networks," Macromolecules **51**, 2517–2525 (2018).

[22] Tang, S., M. Wang, and B. D. Olsen, "Anomalous self-diffusion and sticky Rouse dynamics in associative protein hydrogels," J. Am. Chem. Soc. **137**, 3946–3957 (2015).

[23] Jiang, N., H. Zhang, P. Tang, and Y. Yang, "Linear viscoelasticity of associative polymers: Sticky Rouse model and the role of bridges," Macromolecules **53**, 3438–3451 (2020).

[24] Rouse, P. E., "A theory of the linear viscoelastic properties of dilute solutions of coiling polymers," J. Chem. Phys. **21**, 1272–1280 (1953).

[25] Hansen, D. R., and M. Shen, "Viscoelastic retardation time computations for homogeneous block copolymers," Macromolecules **8**, 343–348 (1975).

[26] Groot, R. D., and W. G. M. Agterof, "Dynamic viscoelastic modulus of associative polymer networks: Off-lattice simulations, theory and comparison to experiments," Macromolecules **28**, 6284–6295 (1995).

[27] Hoy, R. S., and G. H. Fredrickson, "Thermoreversible associating polymer networks. I. Interplay of thermodynamics, chemical kinetics, and polymer physics," J. Chem. Phys. **131**, 224902 (2009).

[28] Amin, D., A. E. Likhtman, and Z. Wang, "Dynamics in supramolecular polymer networks formed by associating telechelic chains," Macromolecules **49**, 7510–7524 (2016).

[29] Wilson, M., A. Rabinovitch, and A. R. C. Baljon, "Computational study of the structure and rheological properties of self-associating polymer networks," Macromolecules **48**, 6313–6320 (2015).

[30] Omar, A. K., and Z. G. Wang, "Shear-induced heterogeneity in associating polymer gels: Role of network structure and dilatancy," Phys. Rev. Lett. **119**, 117801 (2017).

[31] Furuya, T., and T. Koga, "Molecular simulation of structure formation and rheological properties of mixtures of telechelic and monofunctional associating polymer," J. Polym. Sci. Pt. B Polym. Phys. **56**, 1251–1264 (2018).

[32] Amin, D., and Z. Wang, "Nonlinear rheology and dynamics of supramolecular polymer networks formed by associative telechelic chains under shear and extensional flows," J. Rheol. **64**, 581–600 (2020).

[33] Kremer, K., and G. S. Grest, "Dynamics of entangled linear polymer melts: A molecular-dynamics simulation," J. Chem. Phys. **92**, 5057–5086 (1990).

[34] Auhl, R., R. Everaers, G. S. Grest, K. Kremer, and S. J. Plimpton, "Equilibration of long chain polymer melts in computer simulations," J. Chem. Phys. **119**, 12718–12728 (2003).

[35] Eisenberg, A., "Clustering of ions in organic polymers: A theoretical approach," Macromolecules **3**, 147–154 (1970).

[36] Eisenberg, A., B. Hird, and R. B. Moore, "A new multiplet-cluster model for the morphology of random ionomers," Macromolecules **23**, 4098–4107 (1990).

[37] Sontjens, S. H. M., R. A. E. Renken, G. M. L. van Gemert, T. A. P. Engels, A. W. Bosman, H. M. Janssen, L. E. Govaert, and F. P. T. Baaijens, "Thermoplastic elastomers based on strong and well-defined hydrogen-bonding interactions," Macromolecules **41**, 5703–5708 (2008).

[38] Frischknecht, A. L., B. A. Paren, L. R. Middleton, J. P. Koski, J. D. Tarver, M. Tyagi, C. L. Soles, and K. I. Winey, "Chain and ion dynamics in precise polyethylene ionomers," Macromolecules **52**, 7939–7950 (2019).
[39] Hall, L. M., M. J. Stevens, and A. L. Frischknecht, "Dynamics of model ionomer melts of various architectures," Macromolecules **45**, 8097–8108 (2012).
[40] Lu, K., J. F. Rudzinski, W. G. Noid, S. T. Milner, and J. K. Maranas, "Scaling behavior and local structure of ion aggregates in single-ion conductors," Soft Matter **10**, 978–989 (2014).
[41] Lin, K.-J., and J. K. Maranas, "Cation coordination and motion in a poly(ethylene oxide)-based single ion conductor," Macromolecules **45**, 6230–6240 (2012).
[42] Wilson, M., A. Rabinovitch, and A. R. C. Baljon, "Aggregation kinetics of a simulated telechelic polymer," Phys. Rev. E **84**, 061801 (2011).
[43] Mordvinkin, A., D. Döhler, W. H. Binder, R. H. Colby, and K. Saalwächter, "Terminal flow of cluster-forming supramolecular polymer networks: Single-chain relaxation or micelle reorganization?," Phys. Rev. Lett. **125**, 127801 (2020).
[44] Baljon, A. R. C., D. Flynn, and D. Krawzsenek, "Numerical study of the gel transition in reversible associating polymers," J. Chem. Phys. **126**, 044907 (2007).
[45] Perego, A., and F. Khabaz, "Volumetric and rheological properties of vitrimers: A hybrid molecular dynamics and Monte Carlo simulation study," Macromolecules **53**, 8406–8416 (2020).
[46] Beers, K. M., and N. P. Balsara, "Design of cluster-free polymer electrolyte membranes and implications on proton conductivity," ACS Macro Lett. **1**, 1155–1160 (2012).
[47] Kirkmeyer, B. P., R. A. Weiss, and K. I. Winey, "Spherical and vesicular ionic aggregates in Zn-neutralized sulfonated polystyrene ionomers," J. Polym. Sci. Pt. B Polym. Phys. **39**, 477–483 (2001).
[48] Jangizehi, A., M. Ahmadi, and S. Seiffert, "Dynamics of supramolecular associative polymer networks at the interplay of chain entanglement, transient chain association, and chain-sticker clustering," J. Polym. Sci. Pt. B Polym. Phys. **57**, 1209–1223 (2019).
[49] Wu, S. L., S. Liu, Z. J. Zhang, and Q. Chen, "Dynamics of telechelic ionomers with distribution of number of ionic stickers at chain ends," Macromolecules **52**, 2265–2276 (2019).
[50] Brassinne, J., A. Cadix, J. Wilson, and E. van Ruymbeke, "Dissociating sticker dynamics from chain relaxation in supramolecular polymer networks—The importance of free partner!," J. Rheol. **61**, 1123–1134 (2017).
[51] Everaers, R., S. K. Sukumaran, G. S. Grest, C. Svaneborg, A. Sivasubramanian, and K. Kremer, "Rheology and microscopic topology of entangled polymeric liquids," Science **303**, 823–826 (2004).
[52] Hsu, H.-P., and K. Kremer, "Static and dynamic properties of large polymer melts in equilibrium," J. Chem. Phys. **144**, 154907 (2016).
[53] Anderson, J. A., C. D. Lorenz, and A. Travesset, "General purpose molecular dynamics simulations fully implemented on graphics processing units," J. Comput. Phys. **227**, 5342–5359 (2008).
[54] Glaser, J., N. Trung Dac, J. A. Anderson, P. Lui, F. Spiga, J. A. Millan, D. C. Morse, and S. C. Glotzer, "Strong scaling of general-purpose molecular dynamics simulations on GPUs," Comput. Phys. Commun. **192**, 97–107 (2015).
[55] Rubinstein, M., and R. H. Colby, *Polymer Physics* (Oxford University, New York, 2003).
[56] Tanaka, F., and S. F. Edwards, "Viscoelastic properties of physically crosslinked networks: Part 2. Dynamic mechanical moduli," J. Non-Newtonian Fluid Mech. **43**, 273–288 (1992).
[57] Winne, J. M., L. Leibler, and F. E. Du Prez, "Dynamic covalent chemistry in polymer networks: A mechanistic perspective," Polym. Chem. **10**, 6091–6108 (2019).
[58] Von Meerwall, E. D., H. Lin, and W. L. Mattice, "Trace diffusion of alkanes in polyethylene: Spin-echo experiment and Monte Carlo simulation," Macromolecules **40**, 2002–2007 (2007).
[59] Von Meerwall, E., E. J. Feick, R. Ozisik, and W. L. Mattice, "Diffusion in binary liquid n-alkane and alkane-polyethylene blends," J. Chem. Phys. **111**, 750–757 (1999).
[60] Von Meerwall, E., S. Beckman, J. Jang, and W. L. Mattice, "Diffusion of liquid n-alkanes: Free-volume and density effects," J. Chem. Phys. **108**, 4299–4304 (1998).
[61] Durand, M., H. Meyer, O. Benzerara, J. Baschnagel, and O. Vitrac, "Molecular dynamics simulations of the chain dynamics in monodisperse oligomer melts and of the oligomer tracer diffusion in an entangled polymer matrix," J. Chem. Phys. **132**, 194902 (2010).
[62] Kuo, C.-S., R. Bansil, and C. Konak, "Tracer diffusion of flexible probe macromolecules at the sol-gel transition," Macromolecules **28**, 768–770 (1995).
[63] Lewis, C. L., K. Stewart, and M. Anthamatten, "The influence of hydrogen bonding side-groups on viscoelastic behavior of linear and network polymers," Macromolecules **47**, 729–740 (2014).
[64] Zhang, Z., C. Huang, R. A. Weiss, and Q. Chen, "Association energy in strongly associative polymers," J. Rheol. **61**, 1199–1207 (2017).
[65] Rapp, P. B., A. K. Omar, B. R. Silverman, Z.-G. Wang, and D. A. Tirrell, "Mechanisms of diffusion in associative polymer networks: Evidence for chain hopping," J. Am. Chem. Soc. **140**, 14185–14194 (2018).
[66] Colby, R. H., X. Zheng, M. H. Rafailovich, J. Sokolov, D. G. Peiffer, S. A. Schwarz, Y. Strzhemechny, and D. Nguyen, "Dynamics of lightly sulfonated polystyrene ionomers," Phys. Rev. Lett. **81**, 3876–3879 (1998).
[67] Ramirez, J., S. K. Sukumaran, B. Vorselaars, and A. E. Likhtman, "Efficient on the fly calculation of time correlation functions in computer simulations," J. Chem. Phys. **133**, 1–12 (2010).
[68] Doi, M., *Introduction to Polymer Physics* (Oxford University, 1996).
[69] Zhong, M., R. Wang, K. Kawamoto, B. D. Olsen, and J. A. Johnson, "Quantifying the impact of molecular defects on polymer network elasticity," Science **353**, 1264–1268 (2016).
[70] Goldansaz, H., C.-A. Fustin, M. Wubbenhorst, and E. van Ruymbeke, "How supramolecular assemblies control dynamics of associative polymers: Toward a general picture," Macromolecules **49**, 1890–1902 (2016).
[71] Ahmadi, M., A. Jangizehi, E. van Ruymbeke, and S. Seiffert, "Deconvolution of the effects of binary associations and collective assemblies on the rheological properties of entangled side-chain supramolecular polymer networks," Macromolecules **52**, 5255–5267 (2019).
[72] Golkaram, M., C. Fodor, E. van Ruymbeke, and K. Loos, "Linear viscoelasticity of weakly hydrogen-bonded polymers near and below the sol-gel transition," Macromolecules **51**, 4910–4916 (2018).
[73] Weiss, R. A., and H. Y. Zhao, "Rheological behavior of oligomeric ionomers," J. Rheol. **53**, 191–213 (2009).
[74] Castellano, R. K., R. Clark, S. L. Craig, C. Nuckolls, and J. Rebek, "Emergent mechanical properties of self-assembled polymeric capsules," Proc. Natl. Acad. Sci. U.S.A. **97**, 12418–12421 (2000).
[75] Freitas, L. L. D., and R. Stadler, "Thermoplastic elastomers by hydrogen bonding. 3. Interrelations between molecular parameters and rheological properties," Macromolecules **20**, 2478–2485 (1987).
[76] Kwon, Y., Y. Matsumiya, and H. Watanabe, "Dielectric relaxation of type-A chains undergoing head-to-tail association/dissociation: Difference from head-to-head case and correlation with viscoelastic relaxation," Macromolecules **52**, 8484–8502 (2019).
[77] Watanabe, H., Y. Matsumiya, and Y. Kwon, "Dynamics of Rouse chains undergoing head-to-head association and dissociation: Difference between dielectric and viscoelastic relaxation," J. Rheol. **61**, 1151–1170 (2017).

[78] Webb, M. A., U. Yamamoto, B. M. Savoie, Z.-G. Wang, and T. F. Miller III, "Globally suppressed dynamics in ion-doped polymers," ACS Macro Lett. **7**, 734–738 (2018).

[79] Chompff, A. J., and J. A. Duiser, "Viscoelasticity of networks consisting of crosslinked or entangled macromolecules. I. Normal modes and mechanical spectra," J. Chem. Phys. **45**, 1505–1514 (1966).

[80] Chompff, A. J., and W. Prins, "Viscoelasticity of networks consisting of crosslinked or entangled macromolecules. II. Verification of the theory for entanglement networks," J. Chem. Phys. **48**, 235–243 (1968).

[81] Hong, S. D., D. Soong, and M. Shen, "Viscoelastic properties of entangled polymers: The transient network model," J. Appl. Phys. **48**, 4019–4025 (1977).

[82] Qiao, X. Y., and R. A. Weiss, "Nonlinear rheology of lightly sulfonated polystyrene ionomers," Macromolecules **46**, 2417–2424 (2013).

[83] Huang, C. W., Q. Chen, and R. A. Weiss, "Nonlinear rheology of random sulfonated polystyrene iononners: The role of the sol-gel transition," Macromolecules **49**, 9203–9214 (2016).

[84] Feldman, K. E., M. J. Kade, E. W. Meijer, C. J. Hawker, and E. J. Kramer, "Model transient networks from strongly hydrogen-bonded polymers," Macromolecules **42**, 9072–9081 (2009).

[85] Rico-Valverde, J. C., and E. J. Jimenez-Regalado, "Synthesis, characterization and rheological properties, as a function of temperature, of three associative polymers with different microstructure obtained by solution polymerization," Polym. Bull. **62**, 57–67 (2009).

[86] Regalado, E. J., J. Selb, and F. Candau, "Viscoelastic behavior of semidilute solutions of multisticker polymer chains," Macromolecules **32**, 8580–8588 (1999).

[87] Volpert, E., J. Selb, and F. Candau, "Influence of the hydrophobe structure on composition, microstructure, and rheology in associating polyacrylamides prepared by micellar copolymerization," Macromolecules **29**, 1452–1463 (1996).

[88] Golkaram, M., and K. Loos, "A critical approach to polymer dynamics in supramolecular polymers," Macromolecules **52**, 9427–9444 (2019).

[89] See supplementary material at https://www.scitation.org/doi/suppl/10.1122/8.0000218 for the description of LJ units, some details about the simulation model, numerical methods in characterization, tracer diffusion behavior, modulus and segmental diffusion functions for the rest of associative parameters, discussion on the effective chain center, and the effect of random localization of stickers, as mentioned in the context.